ADHESION ENHANCEMENT OF DIAMOND COATINGS ON WC-Co SUBSTRATES THROUGH INTERLAYER DESIGN

A Thesis Submitted to the College of

Graduate Studies and Research

In Partial Fulfillment of the Requirements

For the Degree of Master of Science

In the Department of Mechanical Engineering

University of Saskatchewan

Saskatoon

By

Fan Ye

PERMISSION TO USE

In presenting this thesis in partial fulfillment of the requirements for a Postgraduate degree from the University of Saskatchewan, I agree that the Libraries of this University may make it freely available for inspection. I further agree that permission for copying of this thesis in any manner, in whole or in part, for scholarly purposes may be granted by Professor Q. Yang and Professor A. Odeshi who supervised my thesis work or, in their absence, by the Head of the Department or the Dean of the College in which my thesis work was done. It is understood that any copying or publication or use of this thesis or parts thereof for financial gain shall not be allowed without my written permission. It is also understood that due recognition shall be given to me and to the University of Saskatchewan in any scholarly use which may be made of any material in my thesis.

Requests for permission to copy or to make other uses of materials in this thesis in whole or part should be addressed to:

Head of the Department of Mechanical Engineering
57 Campus Drive
University of Saskatchewan
Saskatoon, Saskatchewan S7N 5A9 Canada

OR

Dean
College of Graduate Studies and Research
University of Saskatchewan
107 Administration Place
Saskatoon, Saskatchewan S7N 5A2 Canada

ABSTRACT

Diamond coating with sufficient adhesion on WC-Co cutting tools is expected to significantly increase their cutting performance. However, the adhesion is always limited by the formation of graphitic soot in the interface due to the catalytic effect of Co on graphite formation. Moreover, the low nucleation density and the high thermal stress in the coatings also result in poor adhesion.

The introduction of interlayer is one of the available approaches to enhance the coating-substrate interfacial adhesion. The goal of this project is to improve the adhesion through the optimization of interlayer design. The Al_2O_3 and Ta mono-interlayer, Al-Al_2O_3, Al-AlN, Al_2O_3-Ta and Al-Ta duplex interlayer systems have been developed in this study. These interlayer materials were prepared using a magnetron sputtering method, and diamond coating were deposited on them using microwave plasma enhanced chemical vapor deposition. In addition, different diamond seeding conditions have been studied to increase the diamond nucleation density. Grazing incident X-ray diffraction was carried out to determine the phase components in the Al-Al_2O_3 and Al-AlN interlayers. Raman spectroscopy and scanning electron microscopy were used to evaluate the quality, morphology and microstructure of the deposited diamond coatings. Rockwell C indentation testing was performed to evaluate the adhesion of the coatings. To elucidate the coating failure mechanism, the compositions around the delaminated spots of diamond coatings after indentation were identified by Energy-dispersive X-ray spectroscopy. To evaluate the tribological properties of the diamond coatings, the diamond coated WC-Co sheets were rubbed against steel and alumina balls respectively.

The results show that continuous diamond coatings were achieved on Al_2O_3, Al-Al_2O_3, Al-AlN and Al-Ta interlayered substrates, whereas a graphite layer was still formed with the Ta monolayer or Al_2O_3-Ta duplex layer accompanied by an easy spallation of diamond coatings. The Al interlayer has played an important role in obtaining high purity diamond by in-situ forming an alumina barrier layer. Especially, the diamond coating deposited with an Al-AlN interlayer exhibits superior interfacial adhesion in comparison with all the other interlayers. Meanwhile, seeding with nano-diamond particles is more efficient than micro-diamond particles for improving the diamond nucleation density on Al-AlN interlayered substrates. Furthermore, the diamond coated WC-Co sheets possess lower coefficient of friction and wear rate than bare sheets when rubbing against either steel or alumina balls.

ACKNOWLEDGEMENTS

Foremost, I would like to express my gratitude to my supervisor Prof. Qiaoqin Yang and my co-supervisor Prof. Akindele G. Odeshi for their continuous instruction and encouragement. I would also like to appreciate my other advisory committee members, Prof. Jerzy A. Szpunar and Prof. Duncan Cree for their insightful comments.

My sincere thanks also go to my group colleagues, Dr. Yuanshi Li, Dr. Chunzi Zhang, Dr. Haidong Wang, Xiaoyu Sun for their insight discussion of my research, and Dr. Lezhi Yang, Santu Bhattacharya, Parisa Ashtijoo and Sheida Shiri for their instruction of the experiments and many other related assistance.

Meanwhile, I am also grateful to Mr. Nanfang Zhang and Mr. Rob Peace in the department of mechanical engineering, Mr. David McColl in the plasma physics laboratory, Mr. Jason Maley in the Saskatchewan Structural Sciences Center, Dr. Chang-Yong Kim in the Canadian Light Source Inc. for their technical support for my experiments.

I finally would like give my special thanks to the financial supporting from the Natural Sciences and Engineering Research Council of Canada (NSERC), the Canada Foundation for Innovation (CFI), and the University of Saskatchewan.

DEDICATION

This work is dedicated to my parents Zhixiang Ye, Yingjun Zhang

&

My brother Terry Ye

TABLE OF CONTENTS

Page

LIST OF TABLES

Table Number Page

LIST OF FIGURES

Figure Number Page

LIST OF ABBREVIATIONS

ASTM	American Society for Testing Material
BEI	Backscattered electron image
BEN	Bias enhanced nucleation
BSE	Backscattered electrons
COF	Coefficient of friction
CRT	Cathode ray tube
CVD	Chemical vapor deposition
DC	Direct current
DLC	Diamond like carbon
EDS	Energy-dispersive X-ray spectroscopy
FCC	Face center cubic
FWHM	Full-width half-maximum
GIXRD	Grazing incident X-ray diffraction
HFCVD	Hot filament chemical vapor deposition
HXMA	Hard X-ray Microanalysis
MPCVD	Microwave plasma enhanced chemical vapor deposition
RF	Radial frequency
RMS	Root mean square
SE	Secondary electron

SEI	Secondary electron image
SEM	Scanning electron microscopy
WC-Co	Cobalt cemented tungsten carbide
WDS	Wavelength-dispersive X-ray spectroscopy
XRD	X-ray diffraction

CHAPTER 1

INTRODUCTION

1.1 Research Motivation

Since the middle of last century, technological innovations in the industrial sector including automobile, aerospace, electrical industries trigger the need for emergence of new materials such as improved aluminum and copper alloys, fiber reinforced polymers, advance glasses and ceramics. The need for extremely high abrasive and wear resistance of these materials drives the development of cutting tools.

Chemical vapor deposition (CVD) diamond opens up the new era for development of high performance cutting tool materials. Owing to its unique crystal and bonding structure, diamond attracts high attention and offers many advantaged properties over other materials, which include ultrahigh hardness, low friction coefficient, high wear resistance, high thermal conductivity and chemical inertness [1]. Combination of these properties makes diamond a promising candidate coating material for conventional cutting tools.

Carbide cutting tools were developed in 1930s and are usually applied in high speed cutting operation because of their high elastic modulus, high thermal conductivity and high hardness over a wide range of temperatures [2]. One typical carbide tool is tungsten carbide insert consisting of WC and Co, in which WC grains are bonded in Co matrix during sintering process. Commercially available WC cutting tools usually contain at least 6 wt. % Co. The amount of Co determines the mechanical properties of the carbide tools. With an increase in Co concentration, the toughness of the cutting tools is improved, but the hardness and the wear resistance deteriorate. The development of CVD diamond coatings makes it possible for high Co carbide cutting tools to maintain the outstanding wear resistance and hardness without sacrificing the toughness.

However, directly deposited diamond coatings on WC cutting tools always face the problem of poor interfacial adhesion, primarily caused by the catalytic effect of Co in the cutting tools [3], which facilitates the formation of graphite soot at the interface. The adhesion is also restricted by low nucleation density and thermal expansion mismatch between the diamond coatings and the WC substrates, which introduces thermal stress inside the coatings during deposition process and leads to the crack or delamination of the coatings.

Surface pretreatment is one of the available methods that can efficiently improve the adhesion of coatings on the substrates. One easy way to improve the nucleation density of diamond is to use the diamond powders to scratch the surface of substrate [4]. The scratches or other defects formed on the surface and the diamond powders imbedded in the surface can provide diamond nucleation sites. Etching is another way of surface pretreatment [5–7]. Acid etching, including HCl, HNO_3 and H_2SO_4 is applied to remove the Co from the substrate surface. The Murakami's Solution ($K_3[Fe(CN)_6]:KOH:H_2O=1:1:10$) is able to etch the tungsten carbide grains on the surface and thus increase the surface roughness [8, 9]. The rough surface has the positive effect on adhesion improvement due to the mechanical locking. Different surface pretreatment methods are usually carried out together to optimize substrate-coating adhesion. However the removal of Co from the surface cannot thoroughly solve the catalytic issue of Co. The Co in the deeper bulk would diffuse upwards to the surface during the CVD process at the high processing temperatures [10]. Additionally, the decrease of Co concentration in carbide cutting tools would definitely results in decrease in toughness. Moreover, the waste recycle of the chemicals is an extra expense for manufacturers and may cause environmental pollutions as well.

Another way to improve the adhesion of diamond coatings on carbide tools is the application of interlayers. Adhesion enhancement can be achieved if the interlayer can suppress the formation of graphite soot by isolating the Co from the carbon-containing precursors, increase the nucleation density of diamond and reduce the thermal stress.

One kind of interlayer is refractory metals such as W, Mo, Nb, Ti, Ta, Cr [11–15]. These materials are able to react with the carbon precursors during diamond deposition to form carbides which provide nucleation sites for diamond growth. The chemical bonds between the carbides and the diamond coatings enhance the adhesion as well. Another kind of interlayer is refractory metallic nitride or carbide such as TiN, TaN, TiC, CrN, ZrN, ZrC, NbC, TiCN [16–21]. These materials attract people's eyes because they can suppress the diffusion of Co. SiC is another interlayer material [22, 23]. It is revealed that the SiC can react with Co to form CoSi compound, which restricts the catalytic effect of Co on graphite formation.

Neither single metallic layer nor ceramic layer can suppress the diffusion of Co, increase nucleation density and reduce thermal expansion mismatch at same time. Increasing research attentions are currently focused on the design and use of multiple interlayers [24, 25]. The most common design is adding a metallic layer on top of ceramic layer. The metallic layer is expected to enhance the nucleation while the ceramic layer will suppress the diffusion of Co. However the thickness of these multilayer design is usually above 1 µm, which will affect the sharpness of the cutting tools. And the interfaces between interlayers can also experience weak adhesion.

In order to overcome this problem, it is necessary to continue optimizing the interlayer design. The previous work in our group has demonstrated that an Al interlayer of several tens nanometers thick can greatly improve the adhesion of diamond on steel, copper and WC-Co substrates [26–28]. This was explained by the formation of an amorphous aluminum oxide layer during diamond deposition, which can efficiently suppress the diffusion of carbon and cobalt. However the adhesion of diamond coatings on WC cutting tools is still not enough even though the Al interlayer is applied. Additionally, the Al interlayer is soft and can easily become damaged, thereby requiring another layer on top of Al to protect it. Therefore, the Al-based interlayer is a feasible solution to enhance the adhesion of diamond coatings on WC-Co sheets but the interlayer structure need to be optimized.

1.2 Research Objectives

The overall objective of this thesis is to enhance the adhesion of diamond coatings on WC-Co cutting tools through the design of interlayer and diamond pre-seeding. This overall objective can be achieved through the following specific objectives:

1. To investigate and compare the barrier to Co diffusion between the sputtered Al layer and sputtered Al_2O_3 layer.
2. To design the protective layer on top of Al in order to increase the adhesion of diamond coatings.

3. To evaluate the effect of micro-diamond and nano-diamond powders seeding on diamond nucleation enhancement.
4. To synthesis diamond coatings on WC-Co sheets with improved adhesion and compare the tribological properties with bare WC-Co sheets.

1.3 Methodology

Interlayers were deposited by magnetron sputtering. Diamond coatings were deposited by microwave plasma enhanced chemical vapor deposition (MPCVD). The structure of interlayers were characterized by synchrotron based grazing incident X-ray Diffraction (GIXRD). Morphology of diamond coatings was observed by Scanning Electron Microscopy (SEM). Raman spectroscopy was carried out to determine the quality and micro-structure of the diamond coatings. Rockwell C indentation testing was performed to evaluate the adhesion of the diamond coatings. To elucidate the coating failure mechanism, the composition around the delaminated spots of diamond coatings after indentation was determined by Energy-dispersive X-ray spectroscopy (EDS). Tribometer was used to evaluate the coefficient of friction of diamond coatings and bare WC-Co sheets. Wear rate was calculated based on the wear scar profile measured by profilometer.

1.4 Thesis Organization

This thesis is made of five chapters. Chapter 1 introduces the motivation, objectives and morphology of the research, and the organization of the thesis. Chapter 2 provides the literature review related to the research area, including the fundamentals of diamond, synthesis methods, characterization methods and previous research of diamond coatings on WC-Co sheets. Chapter 3 specifies the experimental methods including detailed parameters. Chapter 4 presents the results and discussion of the research. Chapter 5 contains the summary and conclusion of the research and suggestions for future work.

CHAPTER 2

LITERATURE REVIEW

2.1 Diamond Coatings

2.1.1 Atomic and Crystal Structures of Diamond

Carbon exists in several allotropic form, which include graphite, diamond, graphene, fullerene, carbon nanotubes as well as amorphous carbon. These different carbon allotropes possess different properties due to the differences in their atomic and crystal structures. There are three hybrid carbon bonds, sp, sp^2 and sp^3. In diamond crystal structure, each carbon atom is tetrahedrally bonded with four neighbor carbons through sp^3 hybrid orbital. The angles between every two bonds are same, and are equal to 109°28′. Each sp^3 bond has very small bond length of 0.154 nm and high bond energy of 711 KJ/mol [29].

The crystal structure of diamond is made of two face centered cubic (FCC) lattices. As shown in Fig. 2-1, one lattice is shifted by (a/4, a/4, a/4), where a is the lattice constant of diamond, which is 3.567 Å [30]. The shape of CVD diamond is highly dependent on the deposition temperature and the hydrocarbon concentration which provides carbon atoms during diamond growth. The {100} face of cubic shape lattice (Fig. 2-2) can be observed at high temperature and high hydrocarbon concentration, while the {111} face of octahedral shape lattice (Fig. 2-2) dominates at low temperature and low hydrocarbon concentration [31, 32]. The most common CVD diamond crystals are found with the shape combining both faces.

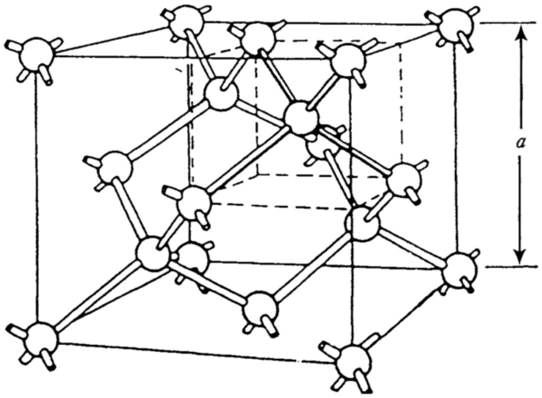

Figure 2-1. Diamond crystal structure [30]

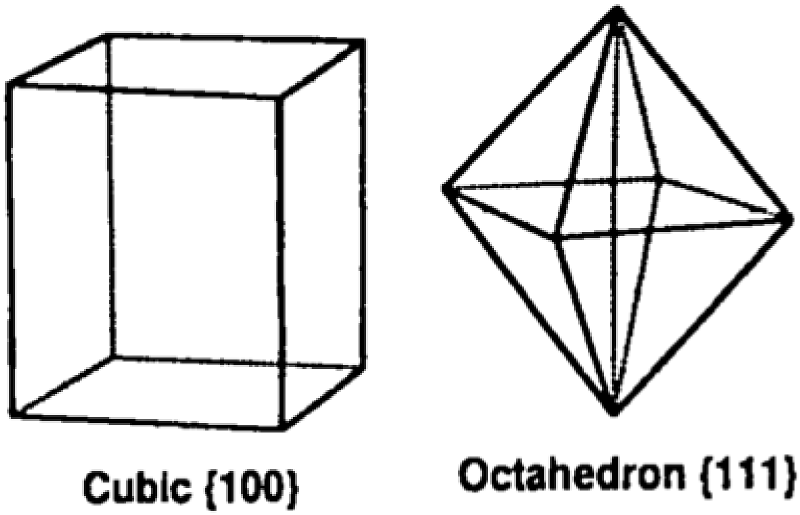

Figure 2-2. Simple crystal shapes of diamond [32]

2.1.2 Atomic and Crystal Structure of Graphite

Graphite is another carbon phase forming during CVD and competing with the growth of diamond. Graphite has continuous hexagonal structures, located in parallel planes, as shown in Fig. 2-3. Each carbon is bonded with three neighbors using sp^2 hybrid bond. The angle between each two bonds is 120°. The sp^2 bond has short length of 0.141 nm and high energy of 524 KJ/mol [29]. The rest electron is located vertically to the plane and coupled with the corresponding electron from adjacent parallel plane to form weaker bond of 7 KJ/mol [29].

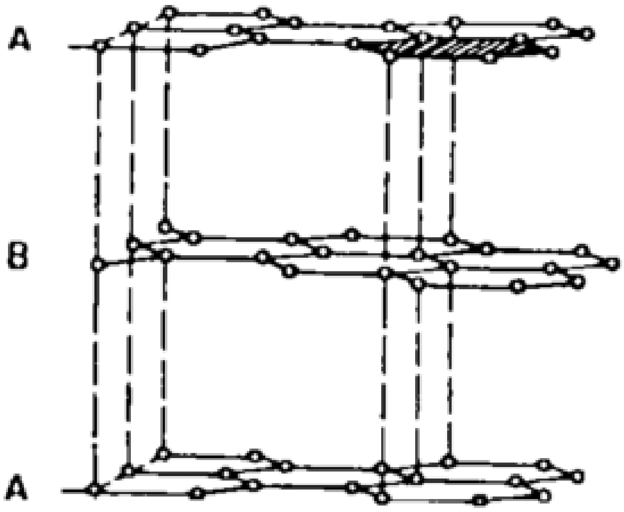

Figure 2-3. Graphite crystal structure [32]

2.2 Synthesis of Diamond Coatings

Synthetic diamond coatings are usually deposited by CVD employing hydrocarbon gases such as methane, ketone and etchant gas such as hydrogen and oxygen to etch non-diamond carbon phases [29, 33]. Among them, methane (CH_4) and hydrogen (H_2) gases are the most commonly used carbon precursor and non-diamond carbon etchant gas. During CVD of diamond, the CH_4/H_2 gas mixture needs to be activated by either external heating (hot filament) or plasma activation [34–36].

2.2.1 Hot Filament Chemical Vapor Deposition

Hot filament chemical vapor deposition (HFCVD), first developed by S. Matsumoto in 1982, is the simplest way to synthesize high quality and continuous diamond coatings [37]. As presented in Fig. 2-4, the CH_4/H_2 gas mixture is fed into the reactor tube made of silica. The filament made of W is heated to around 2000°C to thermally activate the feeding gas. H_2 is dissociated into H atoms and the CH_4 is decomposed into various carbon precursors including CH_3, CH_2 and CH.

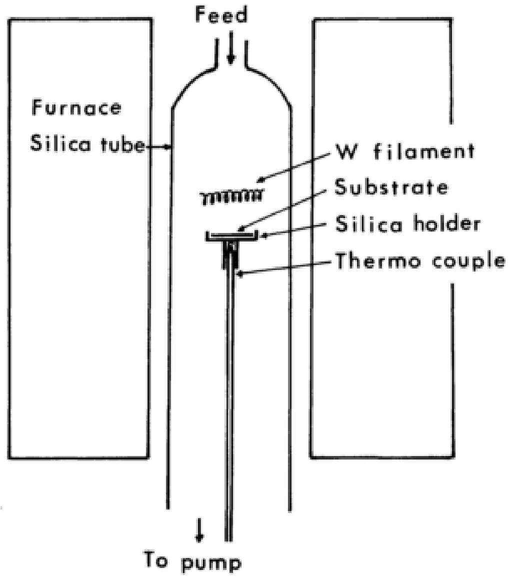

Figure 2-4. Diagram of hot filament chemical vapor deposition [37]

The deposition rate of HFCVD, depending on the deposition conditions such as substrate temperature and gas composition, usually varies from 0.3 to 20 µm/hr [38] . Because of the simple set-up, low cost and easy scale-up, HFCVD is widely used for synthesis of diamond coatings both in academic research and in the industry. However, there are some problems associated with long-term diamond deposition. The most significant problem comes from the filament which is usually made of metals such as W, Mo and Ta. The evaporation of the filament during CVD may contaminate the diamond coatings. Additionally, it is easy for the filament material to react with the hydrocarbon gas to form carbide. The carbide layer covering the filament would influence its stability. Thirdly, the thermal expansion and distortion of the filament during CVD may results in the uneven temperature distribution which may affect the quality of the diamond coatings as well.

2.2.2 Microwave Plasma Enhanced Chemical Vapor Deposition

The research study on diamond synthesis using microwave plasma enhanced chemical vapor deposition (MPCVD) was initiated by M. Kamo [35]. Fig. 2-5 describes the schematic representation of the MPCVD. High frequency microwave (2.45GHz) is generated and guided into reactor made of quartz to discharge plasma. The reflective power should be minimized by adjusting the three tuners and the plunger at the end of the waveguide. A bias can be applied on substrate through a DC generator.

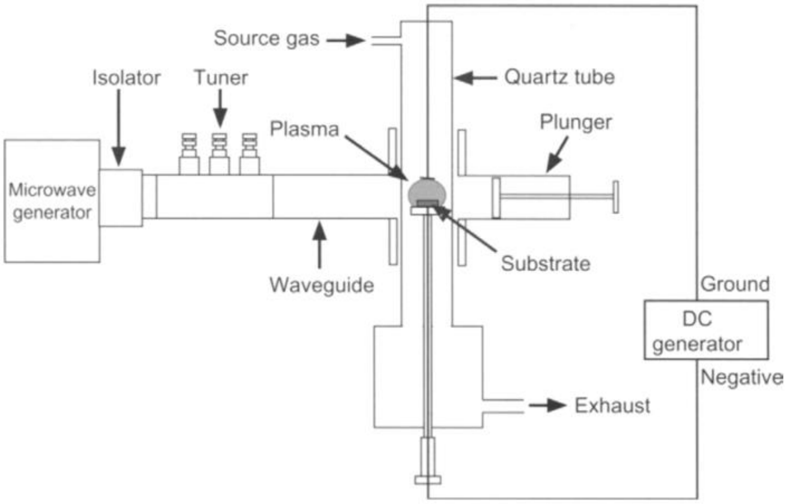

Figure 2-5. Schematic of microwave plasma enhanced chemical vapor deposition [39]

Inside the reactor chamber, the gas molecules are ionized in the plasma discharged by high frequency electric field. The low mass electrons can quickly respond to the change of electric field and thus be accelerated to high energy. The high energy electrons continue to collide with the gas molecules to activate them into atomic hydrogen and reactive carbon precursors for diamond synthesis. Whereas the heavier ions cannot respond to the rapid oscillation of the electric field so that the temperature of the ions and plasma is low. Therefore, the MPCVD could synthesize the diamond coatings at relatively low temperature and increase the energy efficiency. Compared with HFCVD, the MPCVD is favored due to low contamination, higher stability and reproducibility. However, a serious drawback to the use of MPCVD is the low deposition rate and limitation with respect to coating uniformity[40].

2.2.3 Nucleation Mechanism of CVD Diamond

Diamond can be easily grown on diamond surface or cBN surface by CVD due to the identical crystalline structure or small mismatch of the lattice constant [41–43]. However, it is still a challenge to grow diamond on non-diamond surfaces. This challenge can be traced to diamond nucleation. Nucleation is the first step in diamond deposition and would influence the properties of diamond coatings such as grain size, crystalline orientation, surface roughness and transparency. The diamond CVD process can be described in following steps: 1) Incubation. Incubation is a period that the absorbed carbon atoms get supersaturated to generate nuclei. Incubation time varies with the base materials and synthesis conditions. For some materials such as Fe that has high solubility of carbon, the incubation time is very long since more time is required to get supersaturation of carbon on the surface [44] 2) 3-D nucleation on substrate surface. The initial nuclei forms have spherical shape. 3) Termination of nucleation and start of three dimensional growth. The nucleation terminates when the nucleation density reaches a specific value. 4) Faceting and coalescence of the crystallites. Facets appears along with the surface diffusion of carbon. 5) Continuous coating forms and grows [45].

There are two types of nucleation: homogeneous nucleation or heterogeneous nucleation. Even though some homogeneous nucleation cases were found in previous diamond synthesis research [46, 47], heterogeneous nucleation, which is also known as surface nucleation, is still the primary approach for diamond deposition [31]. From the atomistic view, the nucleation process on perfect substrate may be detailed as followings: 1) Atoms from the gas phase are absorbed on the surface. 2) The absorbed atoms may be desorbed into the gas or diffuse over the surface or into the surface. 3) The cluster forms as the surface concentration of adatoms increases. 4) The clusters grow or decay based on the absorption and desorption fluctuation. 5) When the cluster size reaches a critical value, the probability of growth is larger than the decay so that the clusters become stable and continue growth [45].

The problem associated with diamond nucleation comes from two aspects. One is the overlong incubation time for some materials in which carbon has high diffusion rate. Another one is the competing nucleation of non-diamond carbon phases such as graphite. Graphite is the thermodynamically stable phase of carbon materials, whereas diamond is metastable.

To shorten the incubation time and increase the nucleation density, some methods have been tried. One way is the application of carbide forming materials as interlayer. Most of them are refractory metals including Mo, W, Ta, Nb [31]. The generated carbide functions as the nucleation site for diamond deposition. Among them, the nucleation density on Mo surface is highest, probably due to the formation of Mo_2C which works as carbon diffusion barrier so that the carbon concentration on the surface reaches the saturation value sooner [48]. Additionally, the amorphous carbon including diamond-like-carbon and graphite can provide nucleation sites for diamond growth [49], [50]. The second way is to carry out surface pretreatment such as scratching or seeding. The scratching treatment involve the use of abrasive materials such as Al_2O_3, SiC to create defects on the specimen's surface. The defects provide nucleation sites for diamond. The seeding treatment is a specific scratching treatment which uses diamond suspension to ultrasonically scratch the specimen surface. Besides the surface defects caused by diamond powder scratch, some diamond powders would be imbedded into the specimen. The imbedded diamond powders provide initial nuclei for diamond nucleation [51–53]. The nucleation density can be increased to 10^8 cm^{-2} when the Si surface is scratched with diamond powder, and further increased to 10^9-10^{11} cm^{-2} if the Si surface is ultrasonically scratched by diamond powder for several minutes [54]. In a contrast, the nucleation density on Si surface without any treatment is only 10^4 cm^{-2}. Even though both the interlayer and surface scratching or seeding can increase the nucleation density, they cannot control the orientation of the diamond. Bias applied on the substrate is another efficient way to enhance the nucleation density. Yugo [55] firstly reported the bias-enhanced-nucleation (BEN) method in 1991. The nucleation density of diamond on mirror polished Si substrate can reach as high as 10^{10}- 10^{11} cm^{-2} [56]. Moreover, it is found that the diamond can grow heteroepitaxially on Si or SiC surface through the use of BEN [57, 58]. The model built by Yugo suggested that the negative bias increases the energy of the carbon ions impinging the Si surface and thereby increases the bonding strength with the surface because of the ion mixing. The high ions may destroy the weak sp^2 bond as well to suppress the formation of non-diamond phases [59].

2.2.4 Growth Mechanism of CVD Diamond

The reaction inside CVD reactor is complicated. There are a lot of research studies on the mechanism of the gas phase as well as surface reactions, and various detailed kinetic models have been proposed [60–63]. Even though the models differ in detail, they all share some features.

The growth of diamond usually requires the substrate temperature in the range of 1000-1400 K and the hydrocarbon gas such as methane (CH_4) diluted in hydrogen (H_2) rich atmosphere. The hydrogen gas molecules are thermally activated or electrically discharged to form hydrogen atoms (H) or hydrogen ions (H^+), then the hydrocarbon gases are reacted with hydrogen atoms to form carbon precursors consisting of major CH_3 and minor CH_2, CH or carbon dimer.

The previous research findings of Lee [64] has demonstrated that diamond crystals have preferential growth in the <110> direction. The observed face of crystal is usually determined by the face of slow growth. This is why the {100} and {111} faces instead of {110} face [30] are most frequently observed in CVD diamond crystals. Fig. 2-6 shows the possible reaction of diamond growth on {110} face.

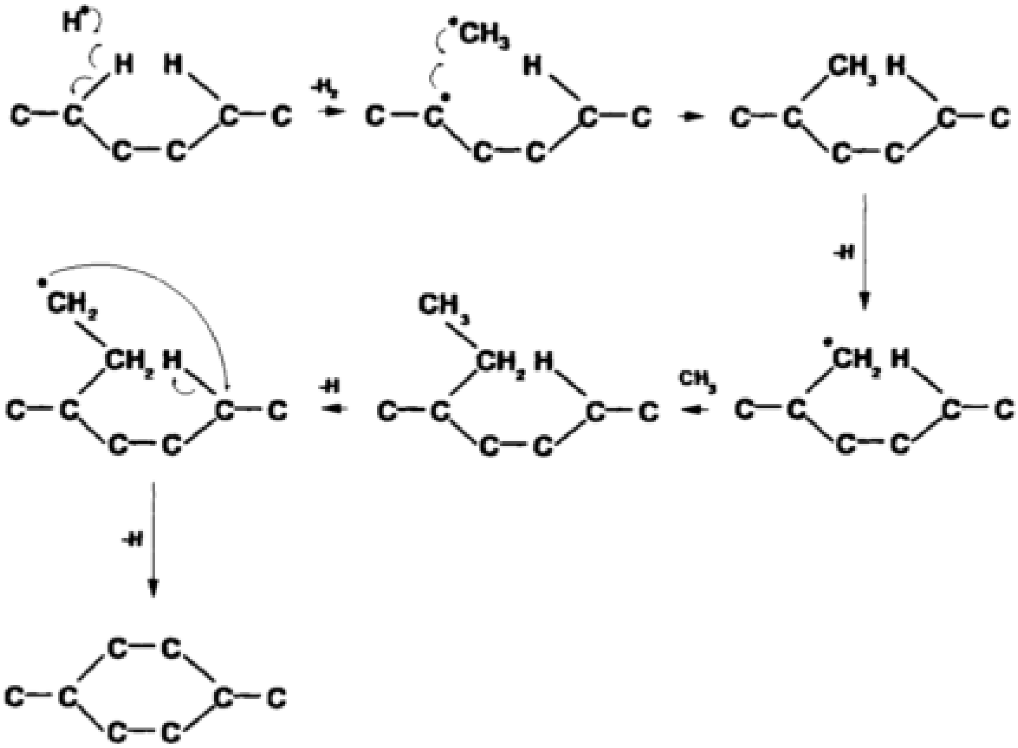

Figure 2-6. Schematic of the possible reaction of diamond growth on {110} face [65]

The free atomic hydrogen abstracts the hydrogen atom from the carbon chain and leaves a radical on the chain. A methyl group ($CH_3\cdot$) is then added on the dangling carbon bond. The repeated process of hydrogen abstraction and methyl group addition elongates the carbon chain. In the final step, the ring is closed indicating the formation of diamond structure [65]. In the summary of the whole process, it is not difficult to notice the critical role of the atomic hydrogen. Firstly, the reaction between hydrogen atoms with the hydrocarbon gases creates the necessary carbon precursors for diamond formation. Secondly the atomic hydrogen abstracts the hydrogen from the carbon chain to create reactive dangling bonds to implant carbon precursors. Thirdly, Hydrogen atoms terminate the dangling carbon bonds and stabilize the diamond structure. Fourthly, the atomic hydrogen etches the graphite 20-30 times faster than the diamond. Therefore the formation of graphite is restricted and only diamond clusters are left on the surface and continue growing [66].

2.3 Magnetron Sputtering

Sputtering technique is widely used nowadays to deposit coatings, including conductive metals or insulated nitride or oxide materials, by choosing appropriate power source. The simplest structure of sputtering is to apply the DC diode between the target and the substrate. The substrate is connected to the anode while the target is connected to the cathode. Ar ions discharged by the high voltage across the diode are accelerated toward the cathode to bombard the target. At the same time, secondary electrons are also emitted from the target, which help to maintain the glow discharge. The sputtered ions move toward the substrate to form films. Sometimes, radio frequency power is used to sputter the insulated target. However, the low deposition rate and the high surface temperature restrict a wider application of DC sputtering [67].

Magnetron sputtering is the dominant method of physical vapor film deposition because of a lot of merits over conventional discharge sputtering. Firstly, the current of magnetron sputtering is one or two order of magnitude higher than simple DC discharge sputtering at the same voltage. Secondly, high deposition rate ranges from 1 nm/s to 10 nm/s can be achieved. Thirdly, the substrate may be kept at low temperature so that it is suitable to deposit temperature sensitive coatings. Fourthly, the working pressure can be reduced to a few millitorr compared with the typical pressure of 100 Pa in DC discharge sputtering. High pressure usually leads to the random collision and scattering of gas molecules and thereby decreases the deposition rate [67, 68]. Fig. 2-7 shows the principle of magnetron sputtering using planar magnetron. In the planar magnetron, one pole is positioned in the central axis of the target while the other pole is formed by placing the magnets around the edge of the target. Then the secondary electrons are trapped in the inhomogeneous magnet field by the Lorentz force which is shown below:

$$\mathrm{F} = \mathrm{e}\,(\mathrm{v} \times \mathrm{B}) \qquad [2.1]$$

Where e is the electron charge, v is the velocity of the electron, B represents the magnetic field. The trapped electrons significantly enhance the possibility of the ionization of argon atoms, thereby increase the sputtering yield of the target and the deposition rate at the substrate [67, 69].

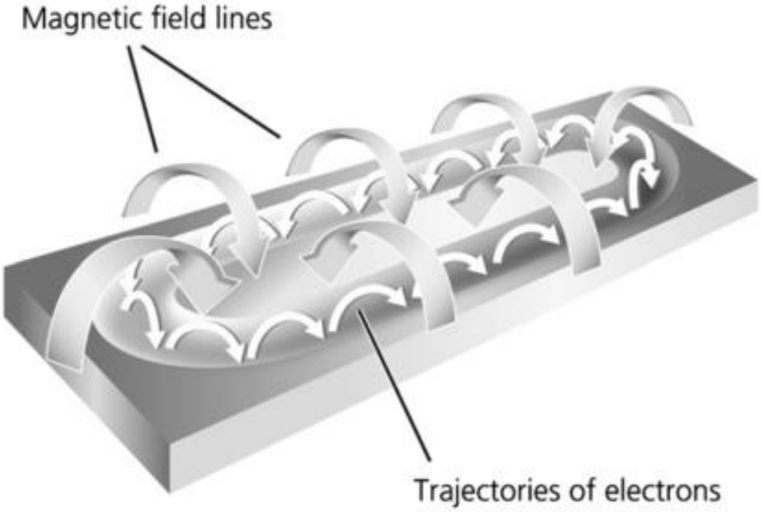

Figure 2-7. principle of planar magnetron [67]

As shown in Fig. 2-7, the plasma discharged by the electrons is confined in the vicinity of the target in the traditional magnetron, which only extends a few centimeter out of the target surface. Therefore, the substrate should be placed inside this region or connected to the negative bias to meet the plasma. However, the ion bombardment would influence the structure and property of the coatings if the substrate is very close to the target. On the other hand, the negative bias on the substrate may increase the defects or stress [69]. This problem can be overcome by the unbalanced magnetron, where the electrons can escape the confinement and reach the substrate by selectively strengthening the magnets poles, as shown in Fig. 2-8.

When the pole at the edge of the target is strengthened relative to the pole at the central axis, the electrons following the field lines are directed to the substrate. Consequently, the plasma escapes the confinement and is expanded to the substrate. The plasma density at the substrate can be increased from the 10^6-10^8 cm^{-3} range to the 10^8-10^{10} cm^{-3} range without the assistant of substrate bias [68]. This magnetron called Type-II unbalanced magnetron was first developed by Windows and Savvides in 1986 [70]. In the Type-I unbalanced magnetron, the pole at the central axis of the target is strengthened relative to the outer pole. The field lines are directed toward the chamber walls so that the plasma density at the substrate is not enhanced [69]. However, O’brien and Arnell successively applied this unbalanced magnetron to deposit chemically reactive porous zirconium coatings [71].

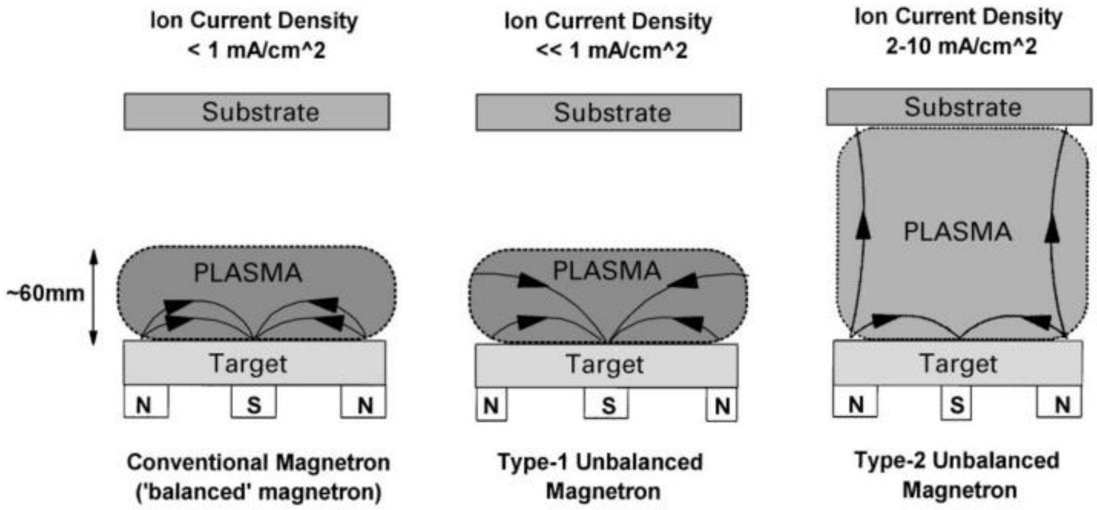

Figure 2-8. Schematic of the plasma confinement of the conventional balanced magnetron and the unbalanced magnetron [69]

2.4 Characterization Techniques

2.4.1 Scanning Electron Microscopy

Scanning Electron Microscopy (SEM) is probably the most widely employed technique to characterize coatings and thin films. Fig. 2-9 describes the typical schematic of SEM [72]. The electrons can be emitted by field emission gun or thermionically emitted from the tungsten or LaB6 cathode filament. After passing through two condenser lens, the emitted electrons are focused to create electron beam with spot size of typically 10 Å in diameter. The double coils at the objective lens are employed to deflect the electron beam linearly along x or y direction over the specimen surface. The energy of the electron beam varies from a few keV to 30 keV [73]. After impinging on the specimen, the primary electron will lose part of energy and transfer it to the specimen. The energy transferred to the specimen may be released in the form of secondary signals including electrons, X-ray, fluorescence, as shown in the Fig. 2-8. The signals can be detected by appropriate detectors then transferred to images through the cathode ray tube (CRT).

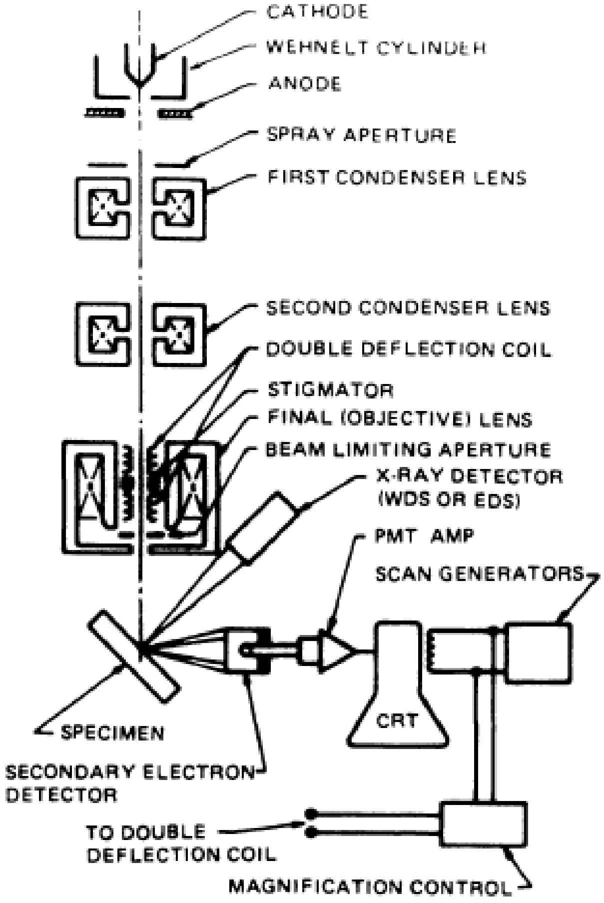

Figure 2-9. Schematic of scanning electron microscopy [72]

Different secondary signals can be collected to present different features of the specimen based on their energy and interaction volume (Fig. 2-10). Secondary electrons (SE) usually have low energy below 50 eV [74]. Therefore, only the secondary electrons from the shallow surface of the specimen can escape and be collected by the detector. Therefore, this signal can create the image with best spatial resolution and present the topographic details of the specimen. Whereas the backscattered electrons (BSE) are generated when the incident electrons experience the elastic scattering with the nuclei of atoms in the specimen so that the energy of the BSE is almost the same with the incident electrons, much higher than SE. Because of the high energy, BSE from deep bulk of the specimen can escape and be detected. Therefore the BSE signal usually provides the chemical composition details of the specimen. Elements of higher atomic mass present brighter contrast in BSE images. X-ray is emitted from the atoms whose inner-shell electrons are excited and the outer-shell electrons jump down to fill the empty orbit. Measuring the energy of X-ray is able to identify the atoms whereas counting the number of the X-ray can determine the concentration of the atoms in the specimen. The instrument based on the X-ray signal, also known as X-ray energy dispersive analysis (EDS), is usually attached to the SEM [73]. If the wavelength other than the energy of the X-ray is analyzed by the detector and dispersed, which is called X-ray wavelength dispersive analysis (WDS), the linewidth resolution in the spectrum can be improved by a factor of 20.

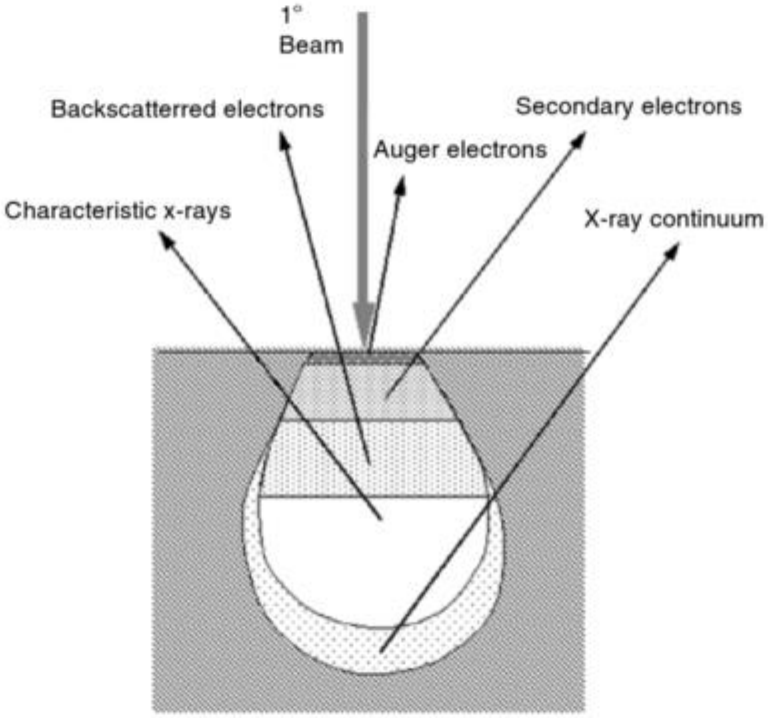

Figure 2-10. Illustration of secondary signals generated after electron beam-specimen interaction [75]

Compared with optical microscope, SEM is capable of imaging at much higher magnification, which can be up to 1,000,000X, and therefore provides extra details besides the topographic information. Additionally, SEM has a larger depth of the field so that most specimen can be focused simultaneously in large area of a rough surface. Therefore, SEM is able to produce high quality images. On the other hand, the quality of the images captured from the optical microscopy is highly dependent on the surface smoothness due to the small depth of the field [74].

2.4.2 Raman Spectroscopy

Raman spectroscopy is usually employed to analyze carbon materials, especially CVD diamond. The origin of Raman spectra comes from the interaction between the incident light (frequency v_0) with the molecules whose bonds have polarizability. When the light illuminates on the specimen, a fraction of the incident light is scattered elastically. This is known as Rayleigh scattering. The frequency of the Rayleigh scattered light is the same with the incident light. Nevertheless, another small fraction of the incident light is scattered inelastically and accompanied with frequency change. The energy transition is illustrated in Fig. 2-11. The frequency of the scattered light decreases to v_0-v_{vib} if the energy transfers from the incident light to the specimen (stokes scattering) or increases to v_0+v_{vib} when the energy transfers to the scattered light from the specimen (anti-stokes scattering). Raman spectra measure the vibrational frequency (v_{vib}) shift of the scattered light with respective to the incident light frequency (v_0) [76].

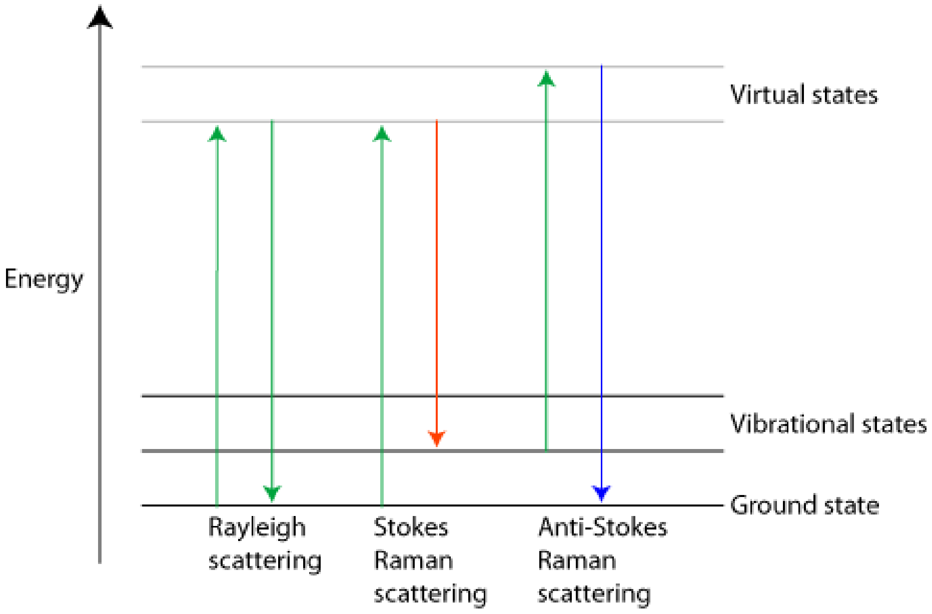

Figure 2-11. Energy transition for elastic and inelastic light scattering
(http://www.doitpoms.ac.uk/tlplib/raman/raman_scattering.php)

The first order peak of the single crystal diamond in Raman spectra is located around 1332 cm^{-1}, which is attributed to the vibration of the two interpenetrating FCC cubic lattices, as mentioned in section 2.1.1. Besides the peak at 1332 cm^{-1}, CVD diamonds always present other peaks which come from other vibration modes due to the impurities. The typical peak locations and their assignment are demonstrated in Table 2-1.

Table 2-1. Assignments for Raman peaks commonly observed in CVD diamonds [77]

Position (cm^{-1})	Typical FWHM (cm^{-1})	Assignment
1100-1150	40-80	Most likely transpolyacetylene at grain boundaries
1332	5-10	first-order diamond Raman line
1345	250	sp2 amorphous carbon (the D peak)
1430-1470	80	Most likely transpolyacetylene at grain boundaries
1520-1580	100	sp2 amorphous carbon (the G peak)

Raman spectrum can be employed to evaluate the quality of the CVD diamond crystals and the residual stress in the diamond coatings. The full-width half-maximum (FWHM) value of the peak located at 1332 cm^{-1} can be considered as a measure of the diamond crystalline quality. The perfect single crystal diamond has the FWHM of 1-3 cm^{-1} [77, 78]. Moreover, the intensity ratio of diamond peak to G peak can be applied to evaluate the phase purity of the CVD diamond crystals [79]. Stress in the CVD diamond coatings may be primarily caused by the thermal expansion difference between the substrate and the coatings, while the mismatch of the crystal lattice can lead to the stress as well. It is very difficult to calculate the extremely accurate stress in the CVD diamond films. Many people have proposed models to calculate the stress from the Raman spectrum [80, 81]. The model proposed by Ager & Drory assumes the biaxial stress in polycrystalline diamond films and uses the Raman peak shift to calculate the residue stress. The calculation of this model varies with the peak splitting conditions. V. Ralchenko [82] simplified the equations in the case of no peak splitting observed in the spectra. The simplified equation is written as below:

$$\sigma(GPa) = -0.567(\nu_{measured} - \nu_0) \qquad [2.2]$$

Where $\nu_{measured}$ and ν_0 represent the measured diamond peak and the standard peak of single crystalline diamond (1332 cm^{-1}).

2.4.3 Grazing Incident X-ray Diffraction

X-ray diffraction (XRD) has long been used to determine the crystallographic structure of crystalline materials. The most straightforward application is to determine the crystal lattice constants to identify the unknown materials. It can also be employed to obtain other information such as crystal orientation, crystal size, defects and stresses. X-ray in the XRD instrument can be produced by bombarding the metal target such as Cu, Co, Fe with high energy electrons. The photon is emitted when the high energy electrons collide with the target atoms and decelerates. The emitted X-ray contains a continuous distribution of energies or wavelengths. However the most important wavelength for analytical purpose comes from the emission of the X-ray photons when the incident electron ejects out the inner-shell electron from the target atom and the outer-shell electron jumps down to the inner shell to fill the empty orbit. In order to separate the desired monochromatic X-ray from the rest, a filter is usually installed to absorb the unwanted X-ray photons. The monochromatic X-ray photons are then converged into narrow X-ray beam. When the X-ray beam comes in contact with the specimen under investigation, it is diffracted by the atoms. Constructive interference occurs between incident and diffracted X-ray beams when the wavelength of the X-ray and the lattice spacing meet specific condition which is called Bragg's Law. The equation of the Bragg's Law is shown below:

$$n\lambda = 2dsin\theta \qquad [2.3]$$

Where d is the lattice spacing, θ is the incident angle of the X-ray, λ is the wavelength of the X-ray photon and n is the integral. The X-ray can penetrate deeply into the materials, typically a few millimeters, providing the information averaged on a large amount of atoms. Therefore the X-ray results of the bulk materials are accurate and precise. However, when it comes to the thin film characterization, the advantage of the conventional XRD becomes disadvantage. The peaks of the thin films usually have low intensity and are unobservable among a bunch of peaks coming from substrate.

The grazing incident x-ray diffraction (GIXRD) is able to avoid the strong scattering from the substrate. Most materials have refractive index less than 1.0 at X-ray energy level. Therefore, completely external reflection can be observed when the incident angle is small enough. At this point, there is still an evanescent X-ray penetrating into the material and scattered from it so that the intensity is highest at the surface [83]. Even though the incident angle (ω) is fixed at a small angle, the diffracted X-ray can be detected at any angles (2θ). By changing the incident angle, the penetration depth can be tuned to characterize the layer of interest. Therefore, it is possible to use GIXRD to obtain the surface information or depth profile of the thin films and detect the stress distribution as a function of the depth.

The synchrotron based GIXRD has many advantages over other cathode tube based GIXRD. The X-ray intensity from synchrotron radiation is much higher, which is very important to measure the weak scattered X-ray from the surface of thin films. Additionally, it is available to select the desired wavelength to avoid fluorescence background and obtain the highest intensity of the possible peaks [84].

2.4.4 Adhesion Test of Hard Coatings

Adhesion refers to the condition in which two close surfaces are jointed together by chemical bonds, or mechanical anchoring or both. The adhesion of coatings on substrates is of significant importance but least understood in surface engineering. It is difficult to precisely define the adhesion since it is affected by material's microstructure, external loading and environmental conditions. The concept of adhesion can be introduced from "basic adhesion" and "practical adhesion" [85]. "Basic adhesion" only refers to the interatomic interactions at the interface of coating and substrate. From the thermodynamic view, the work required to detach coating and substrate at interface can be written as the equation below:

$$W_A = \gamma_f + \gamma_s - \gamma_{fs} \qquad [2.4]$$

Where Υ_f and Υ_s represent the surface energy of the film and the substrate respectively. Υ_{fs} is the interfacial energy. Adhesion occurs only when W_A is positive. From the macroscopic view, besides the strong chemical bonding, van der waals force also contributes to the adhesion and strengthen the joint between coating and substrate [86]. The "practical adhesion" takes into account not only the interatomic bond but also the mechanical properties of the coatings and substrates including toughness and elastic modulus, the distribution of defects such as flaws, pores and other lattice defects, the external loading conditions and the friction behavior against the abrasive components [87].

The practical adhesion is difficult to evaluate since it is greatly influenced by the working conditions. However, there are several approaches to evaluate the adhesion of hard coatings in the laboratory. (1) Scratch test. A Rockwell-shaped diamond indenter or a stylus with known radius of curvature is employed to scratch over the coatings with the linear increasing vertical load, as shown in Fig. 2-12 (a). The scratch scars are then observed under optical microscope or SEM to estimate the critical load that results in the failure at the interface of coating and substrate. Usually the instrument is also equipped with acoustic emission detector which is put on the sample. The acoustic signals are small when the coating adheres to the substrate but become large when the failure at the interface of coating and substrate occurs. Therefore the large acoustic signal can be taken as a measure of the critical load [86]. Even though this method is widely applied to evaluate the adhesion of the hard coatings, it is not suitable for diamond coatings since the small diamond tips may be damaged by the hard diamond coatings.

(2) Four-point bending test. As shown in the Fig. 2-12 (c), the coating is loaded by compressive stress. The failure of the coating is characterized by micro-cracks of the coatings which are detected by acoustic signal [88]. The substrate is not coated near the two load points to avoid the noisy acoustic signals which are not generated by the homogeneous bending of the coating. Unlike the inhomogeneous stress in the scratch test, the homogeneous compressive stress in this way is expected to provide more reliable result.

(3) Impact test [89]. The Fig. 2-12 (b) illustrates the schematic of the impact test which is used to test the fatigue strength of the coating/substrate complex. The sample is loaded cyclically by the ball made of tungsten carbide. The maximum frequency and the load is 50 Hz and 1500 N respectively. The vertical impact load is controlled by the stress gauge. The loading cycles when the damage is firstly observed is recorded as a measure of the adhesion.

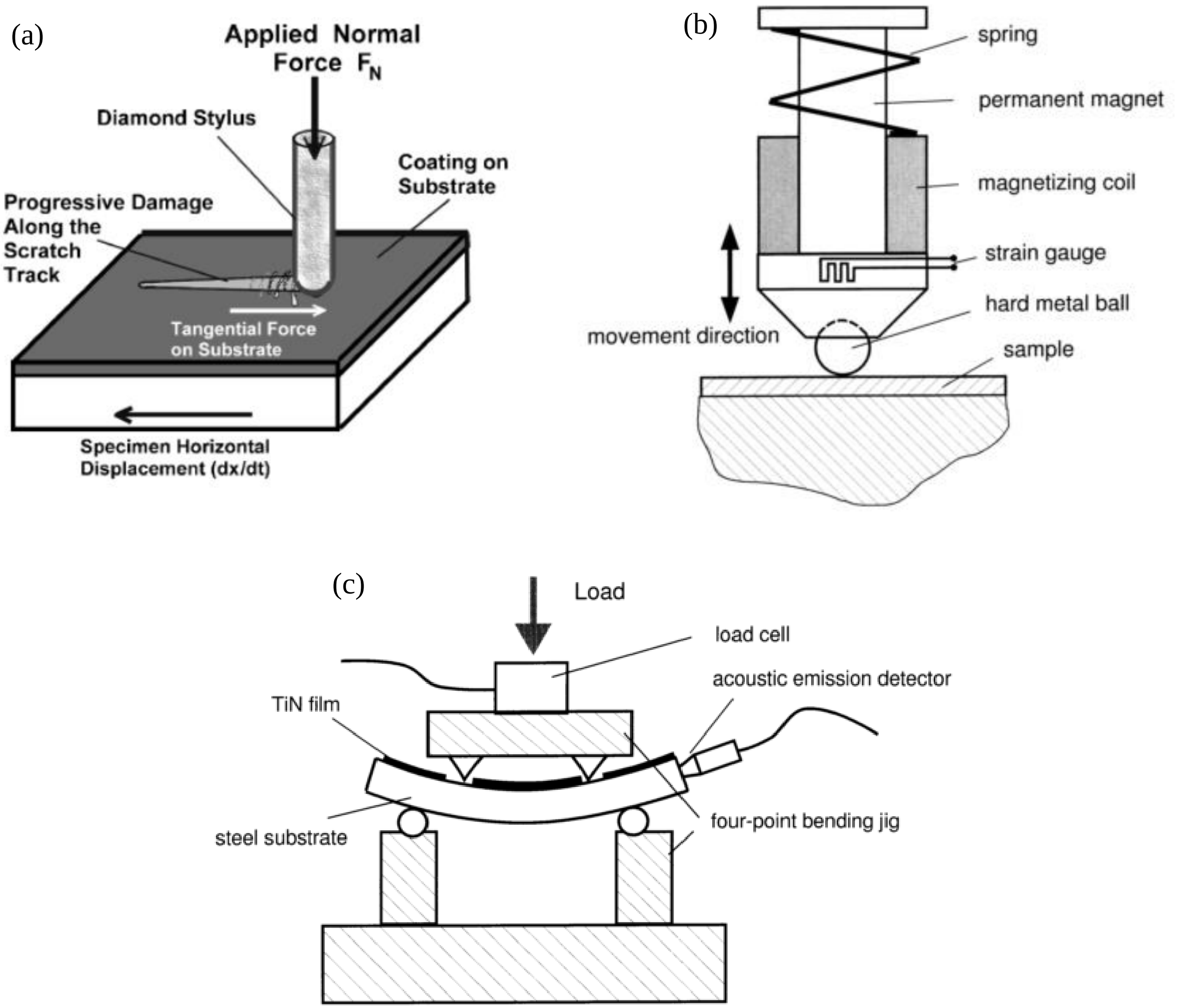

Figure 2-12. Schematic of the adhesion test of (a) scratch test (from ASTM C1624), (b) the impact test, (c) the four-point bending test [89]

(4) Rockwell C indentation test. Rockwell adhesion test, developed by the Union of German Engineers (Verein Deutscher Ingenieure, VDI), is always carried out to evaluate the adhesion of diamond coatings due to the easy operation. A conventional Rockwell tester is equipped with a spherical coned Rockwell C indenter which presses the coatings with high load of 1470 N. The imprint features are observed under microscope to evaluate the adhesion. The damage of the coatings are classified into 6 classes (HF1-6) as shown in Fig. 2-13. In HF 1, only a few cracks are observed in the neighbor of the imprint area. The number of cracks increases in HF 2. In HF 3,

minor delamination is observed around the indentation, and it becomes worse through HF 4 to 5. In HF 6, the coating around the indentation is completely delaminated [90].

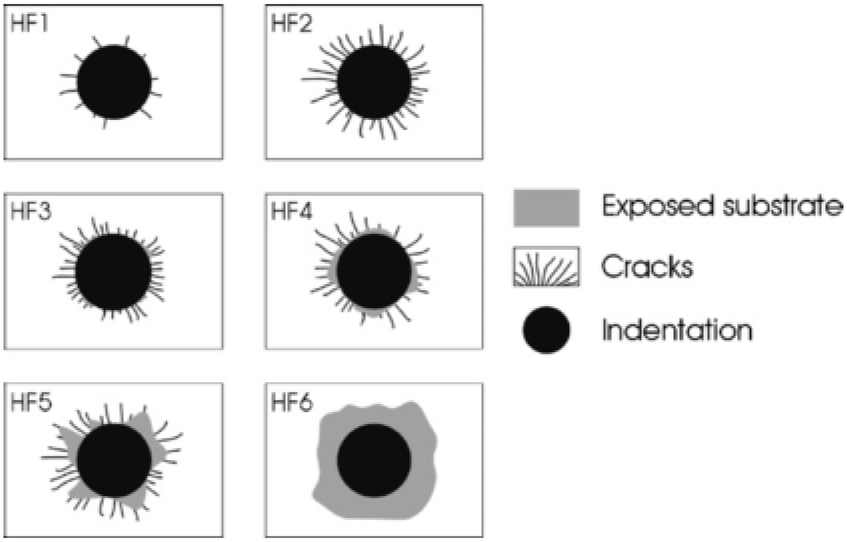

Figure 2-13. Sketches of the damage classes used in Rockwell C indentation test [90]

2.4.5 Wear Test

In general wear refers to the damage of a solid surface caused by the mechanical motion with other contact of solid, liquid or gas. Wear can be classified as lubricated or non-lubricated wear. It can also be classified based on the wear mechanism in different types. The wear mechanism is complicated and one single wear behavior contains probably more than one mechanisms. Fig. 2-14 introduces the classification of the wear based on the relative motion types [91]. The wear caused by sliding movement can be classified as abrasive wear, adhesive wear, fatigue wear, fretting wear and polishing wear. The carbide inserts face the problem of abrasive wear and adhesive wear most. Abrasive wear is the wear caused by the hard particles or protrusions forced against and moving along a solid surface. There are two types of abrasion wear: two-body abrasion and three-body abrasion. The former one happens when the hard particles or protrusions are fixed to one surface and slide along another surface, while the latter one occurs when the abrasive particles are sandwiched between two surfaces [92]. The adhesive wear is the wear that occurs when the material of one surface is transferred to another surface during the relative movement.

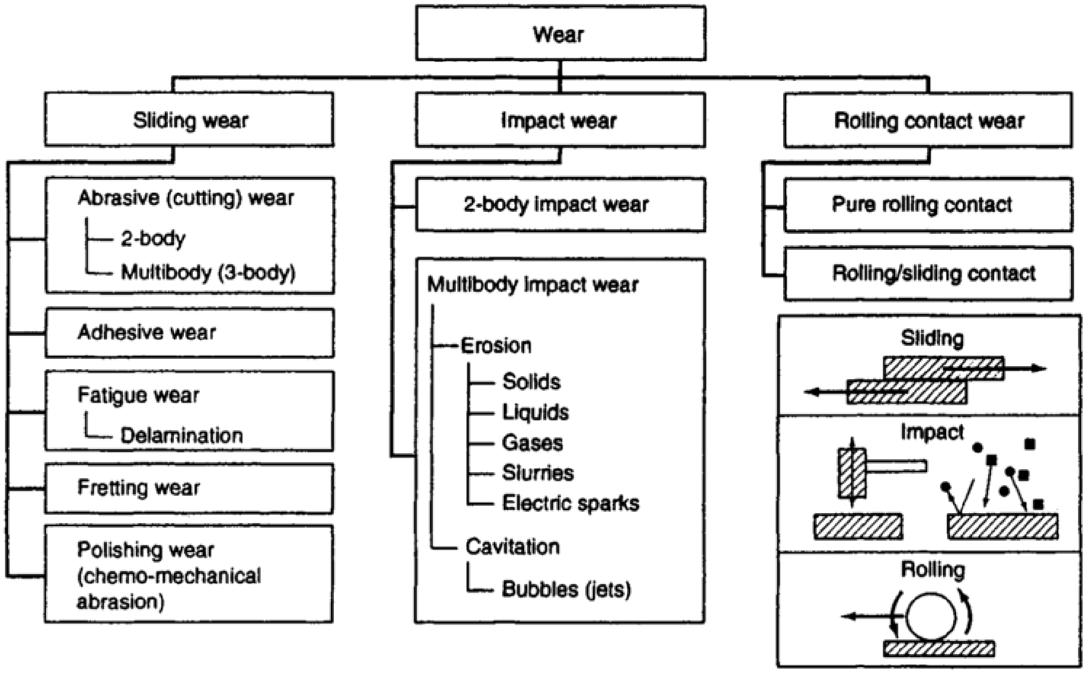

Figure 2-14. Categories of wear classified by the relative motions [91]

There are different wear tests based on various wear mechanisms. The wear performance is a wear system property instead of intrinsic material property like toughness, elastic modulus. In other words, the wear test measures the material's response to one specific wear environment and the result varies under different wear conditions [93]. One general test method to study sliding wear behavior is the pin-on-disk wear test. The configuration of this method is shown in Fig. 2-15. A pin is pressed against the flat disk. The wear scar is generated as the relative motion between disk and pin occurs. Either the pin or disk moves circumferentially. According to ASTM, either the mass loss or volume loss can be used to determine the wear of the materials. The mass loss should be converted to volume loss by dividing the mass loss by the density. For rounded pin, the wear volumes of the pin and the disk can be calculated by the equation 2.5 and 2.6 respectively if there is negligible wear on the counterpart:

$$V = \frac{\pi}{64} \times \frac{W^4}{R} \tag{2.5}$$

$$V = \frac{\pi}{6} \times D \times \frac{W^3}{R} \tag{2.6}$$

Where W is the width of the flat on the pin in equation 2.5 or width of the wear scar in equation 2.6. R is the spherical radius of the pin and D is the radius of the wear scar. In some cases that there is wear on both the pin and the disk, it is more useful to measure the wear depth instead of the wear width.

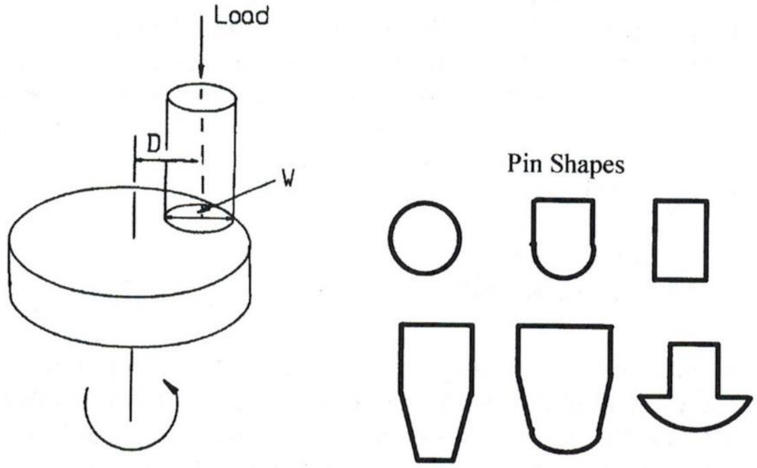

Figure 2-15. Schematic of the pin-on-disk test and the cross-section of the pin [94]

Another general test is the “pin-on-flat” test which is similar with the “pin-on-disk” test. The difference between them is that the pin moves unidirectional and at constant speed in “pin-on-disk” test, but changes direction cyclically and accompanied with acceleration and deceleration in “pin-on-flat” test [94]. The wear test of diamond coated metal or ceramic materials usually adopts either “pin-on-disk” [95–97] or “pin-on flat” test [20, 98, 99] with or without lubricants. The pin or the ball may be chosen from tungsten carbide ball [95], alumina ball [96, 97] or steel [20, 99].

2.4.6 Optical Profilometer

Surface topography and coating thickness are important properties for coating technology. Therefore it is necessary to develop a reliable technique to measure the surface roughness and the coating thickness with high accuracy. Stylus profilometer is an easy and conventional way to measure the surface topography. The surface topographical image is recorded as the stylus slightly presses on the specimen surface and moves across the surface to trace the height variance of the surface. The thickness of the coating can be directly acquired by tracing the height drop at the coating/substrate step. However the accuracy of the stylus profilometer is limited to the dimensions of the stylus. Additionally, the movement of the stylus may scratch the coating surface.

The non-contact optical profilometer based on interferometry has higher accuracy than the stylus profilometer. Fig. 2-16 illustrates the basic structure of the optical profilometer based on interferometry. The beam from the light source is split into two beams. One beam is reflected from the specimen surface while another one is reflected from the reference mirror inside the objective. When two beams are combined, there will be constructive and destructive interferences resulting in the bright and dark bands in the fringe on the surface.

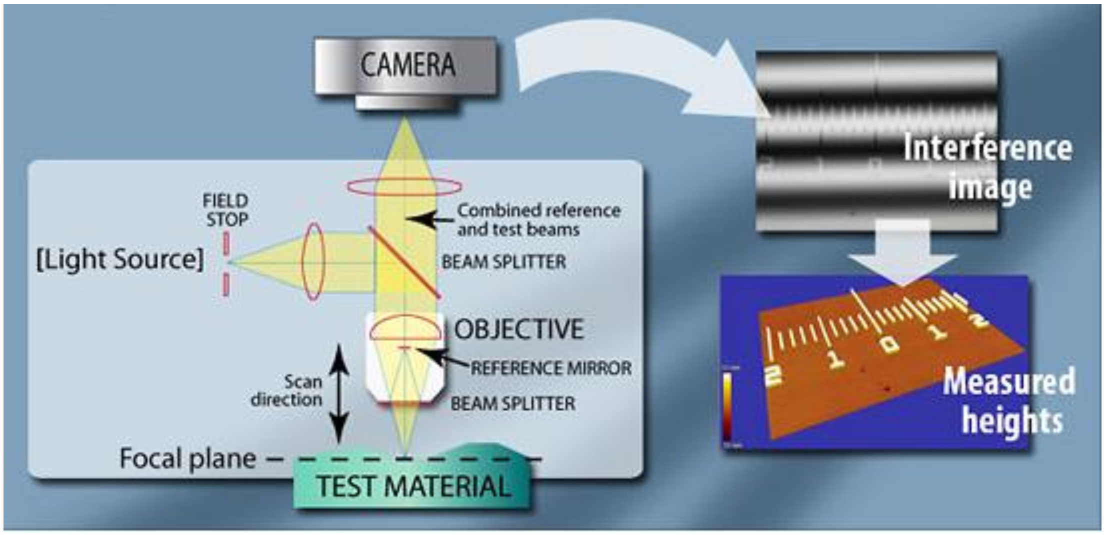

Figure 2-16. Schematic of optical profilometer based on interferometry (From Zygo Co.,)

The constructive interference is the condition when the optical path difference between the reference mirror reflected light and the specimen surface reflected light equals the integral number of the wavelength of the light. Because the reference mirror is close to perfect flat, the optical path difference comes from the height variance of the specimen surface. The accuracy of the optical profilometer may be as high as 1 nm [73].

2.5 Surface Treatment of WC-Co Sheets

WC-Co sheets always face the adhesion problem if the diamond is directly deposited on the surface. As discussed in the Section 1.1, the poor adhesion is caused by three major reasons. The most important reason is the formation of graphite which is catalyzed by Co in the carbide sheets. The other two reasons are the low nucleation density and the thermal stress. To overcome the problem and increase the adhesion, a few surface treatment methods have been employed in past decades. Different surface treatments are focused on different functions.

To increase the nucleation density, the most easy and straightforward way is to use diamond seeding which is to take diamond suspension to ultrasonically scratch the specimen surface. Diamond seeding on WC-Co sheets plays two major roles. One is to increase the roughness and another one is to imbed diamond powders into the substrate. Huang's research [100] indicates the appropriate surface roughness created by diamond micro-scratching is important to increase the adhesion of diamond on cemented WC sheets. Many studies have reported the diamond nucleation enhancement by diamond seeding [4, 8, 101]. Itoh [101] found the diamond nucleation density increases with decreasing grain size of the diamond powder. The optimum range of the diamond powder for seeding is from 0-0.25 µm. Barros investigated dispersion liquid properties on the efficiency of diamond seeding and proposed five important properties: low dipole moment, high vapor pressure, low density, low viscosity and low surface tension [4]. The use of Murakami's solution ($K_3[Fe(CN)_6]:KOH:H_2O=1:1:10$) is another typical method to increase the surface roughness of WC-Co sheets. Murakami's reagent is able to selectively attach the WC grains and hence roughen the surface [8, 9]. In recent years, laser treatment [102–104] was carried out to roughen the surface of WC-Co sheets. Veillère's research [102] reported that the laser treatment can significantly increase the surface roughness of WC-Co sheets and the stress in the coating deposited on them decreases.

The binder phase Co in the cemented WC cutting tools has detrimental effect on the adhesion [105, 106]. Similar with other transition metals whose 3d orbit is partially filled, Co has catalytic effect on the graphite formation during CVD process [107]. Additionally, the solubility of carbon in cobalt is up to 0.2-0.3 wt. % at typical diamond deposition temperature which is around 1000-1400 K. Therefore, carbon in the deposited diamond grains may diffuse into the carbide substrate during CVD and leaves voids at the interface resulting in the deterioration of adhesion strength [108]. Chemical etching is the most commonly used surface treatment method to remove the Co. Many strong oxyacid including HNO_3, H_2SO_4 and H_3PO_4 or hydrochloric acid can etch and oxidize the Co [8, 102, 109, 110]. In order to achieve effective etching result, acid etching is always performed after surface roughing. For example, Caro's acid (H_2SO_4-H_2O_2 solution) is usually applied after first etching using murakami's solution [108, 111]. The quality of diamond deposited on WC-Co substrate treated by combination of laser treatment and acid etching was found better than simply laser treatment as well [102]. Laser treatment is able to not only increase the surface roughness but also selectively evaporate Co phase from the cemented carbide substrate. Co has low melting and boiling point compared with WC so that accurate control of the laser power may evaporate the Co but leave WC grains in solid [104]. Moreover, hydrogen plasma treatment can be incorporated into surface treatment after first step of acid etching. Hydrogen plasma treatment functions to decarbonize the WC grain on surface so that new WC grains form during CVD and deposited diamond crystals can be imbedded inside to increase adhesion [109, 112].

However, the cobalt in the deeper bulk would still diffuse up to the surface at CVD high temperature [10, 108, 113]. Another concern is that the reduced amount of cobalt in the cemented carbide would lead to the debonding of WC grains. As a result, the substrate would get embrittled leading to reduction in lifetime [108].

2.6 Interlayer Design on WC-Co sheets

Similar with the surface treatment, the interlayer designed on WC-Co sheets should meet three basic requirements. The interlayers should have low diffusion coefficient of Co to prevent cobalt reacting with the carbon precursors during CVD, secondly increase the diamond nucleation density, and thirdly have intermediate thermal expansion coefficient to function as thermal expansion buffer layer.

So far many refractory metals [11–15] such as W, Mo, Nb, Ti, Ta, Cr, ceramics [16–21] including TiN, TaN, TiC, CrN, ZrN, ZrC, NbC, TiCN, SiC and amorphous carbon [114] have been employed as interlayer on WC-Co to enhance the adhesion of diamond coatings. These interlayer materials can be categorized based on their specific functions of either diamond nucleation enhancement or Co diffusion barrier. As discussed in Section 2.2.3, refractory metals and amorphous carbon materials are taken into account as interlayer due to high diamond nucleation density on them [31, 48–50, 115]. Additionally, some refractory metal carbide or nitride such as TiC and TiN also functions as diamond nucleation enhancement layer [10, 116]. On the other hand, some nitride materials including CrN, ZrN, NbN, TaN and TiAlN are selected as Co diffusion barrier [17, 18, 117]. Among them, CrN is considered as one of the best interlayers to suppress the diffusion of Co. Hojman [21] observed that all the interstitial sites were fully occupied by N atom in the structure of CrN so the diffusion path for Co or C was restricted. Moreover, SiC has proved to be another outstanding interlayer candidate material. It was revealed that the SiC can react with Co to form cobalt silicide so that the catalytic effect of Co was hindered[22, 23].

In order to ensure the interlayer containing more than one functions, the idea of multiple interlayers [19, 24, 25, 118] was proposed. Different functions of interlayer were assigned to different sublayers. Poulon's group [24, 25] has tested several groups of multiple interlayer. In TaN/Mo or ZrN/Mo interlayer design, TaN and ZrN contribute to suppress the diffusion of Co while Mo was applied to increase the diamond nucleation density. In his another innovative design, TaN/Mo was employed as diamond nucleation enhancement layer, another nine periods of nano-grained TaN and ZrN bilayer was designed as cobalt diffusion barrier. This design elongates the diffusion path of cobalt so that Co diffusion is successfully suppressed. But the preparation methods of this design is complicated and too many interfaces would deteriorate the adhesion between sublayers. Additionally, the multiple interlayers are usually thicker than 1 μm, which would influence the sharpness of the cutting tools

In our group, a lot of research [26–28, 119–125] regarding to the interlayer design for diamond coatings have been conducted. In 2006, Yuanshi [26] first revealed that a slight addition of Al and Si into Fe-Cr alloy can increase the nanocrystalline diamond nucleation and improve the adhesion of diamond to the substrate. Moreover, aluminum [119, 122] was proved to enhance the adhesion of diamond on stainless steel by acting as an individual interlayer or alloying with the steel. In 2010, dual metal interlayers [121] of Al/Cr and Al/Ti were employed on stainless steel, where Al was employed to prevent the formation of graphite, while Cr or Ti was added to improve the diamond nucleation. However continuous diamond coating could not be achieved due to the high thermal stress. Further research [124, 125] demonstrated that an ultrathin Al oxide layer appears during diamond deposition on ferrous substrate alloyed with aluminum. Similar with Co, the transition metal Fe has catalytic effect of graphite formation as well. But the oxidized aluminum layer efficiently blocks the diffusion of both carbon and iron so that the solubility of carbon on the surface is increased and the catalytic effect of iron is restricted. Not restricted in ferrous materials, aluminum interlayer was found to be able to improve the adhesion of diamond coatings on other materials as well including copper and WC-Co [27, 28]. On WC-Co substrate, Al/W multiple interlayer [28] was employed. W was used to increase the diamond nucleation density while Al to suppress the diffusion of Co. Nevertheless, local diamond spallation was still discovered due to the large internal stress.

The internal stress in diamond coatings deposited on WC-Co sheets primarily comes from thermal stress. Thermal stress can be estimated by the equation 2.7, as shown below [80]:

$$\sigma_{thermal} = \frac{E}{1-\nu}\int_{20°C}^{T}(\alpha_c - \alpha_s)dT \qquad [2.7]$$

Where E and ν are the Young's Modulus and the Poisson ratio of the coating. α_c and α_s represent the thermal expansion coefficient of the coating and the substrate, which is 1×10^{-6} $°C^{-1}$ for diamond coating and 4.42×10^{-6} $°C^{-1}$ for WC-Co substrate at 293 K. Therefore, the optimum thermal expansion coefficient of the interlayer is expected to be between diamond coating and WC-Co sheet to reduce the thermal stress in the diamond coating.

CHAPTER 3

EXPERIMENTAL METHODS

3.1 Substrate Materials Preparation

Commercial WC-Co sheets consisting of 6 wt. % of Co purchased from Kennametal Inc. were used as substrates for diamond deposition. The substrates were first polished using #180 and #320 sandpapers sequentially. This was followed by polishing using diamond pastes with grain size of 9 µm, 3µm and 1µm respectively into mirror-like surface. The prepared surfaces were then cleaned with ethanol.

3.2 Interlayer Deposition

The interlayers of Al, AlN, Al_2O_3 and Ta were deposited on polished WC-Co sheets by a magnetron sputtering system manufactured by Plasmionique Inc (Fig. 3-1). The detailed deposition parameters and the thickness of each layer are listed on Table.3-1. The base pressure was 1×10^{-7} torr for all the materials deposition. All the interlayers were deposited under a pressure of 10 mtorr at room temperature. Pure Ar (99.99%) was used to deposit Al and Ta interlayers. While AlN and Al_2O_3 were deposited by sputtering Al target in a mixture of Ar and N_2 gases and a mixture of Ar and O_2 gases respectively.

Table 3-1. Parameters of interlayer deposition

Interlayer	Power Source	Gas Ratio	Deposition Time	Thickness
Al	DC75 W, 130 V	Pure Ar	30 min	60-90 nm
AlN	RF 120 W, 120V	N_2:Ar=13:20	2 hrs	130-150 nm
Al_2O_3	Pulsed DC 50 KHz, 275 W, 280 V	O_2:Ar=1:6	3 hrs	120-140 nm
Ta	RF 75 W, 120 V	Pure Ar	25 min	60-90 nm

Figure 3-1. Magnetron sputtering instrument

3.3 Research of Seeding Conditions on Diamond Nucleation

The optimum seeding conditions varies depending on the different substrates. To investigate the effect of seeding conditions on diamond nucleation of Al-AlN interlayered WC-Co sheet and optimize the seeding parameters, six groups of diamond suspension were designed as shown below:

Group A: 0.5 wt. % nano-diamond powder dispersed in ethanol
Group B: 1 wt. % nano-diamond powder dispersed in ethanol
Group C: 3 wt. % nano-diamond powder dispersed in ethanol
Group D: 0.5 wt. % micro-diamond powder dispersed in ethanol
Group E: 1 wt. % micro-diamond powder dispersed in ethanol
Group F: 3 wt. % micro-diamond powder dispersed in ethanol

The Al-AlN interlayer coated WC-Co sheets were ultrasonically pre-scratched in different diamond suspension groups for 30 seconds, followed by an ultrasonic rinsing in distilled water for 10 minutes. The grain sizes of nano-diamond powders and micro-diamond powders are 3-4 nm and 1 µm respectively.

The seeded samples were then put into a 2.45 Hz microwave plasma enhanced chemical vapor deposition (MPCVD) reactor manufactured by Plasmionique Inc (Fig. 3-2) for diamond nucleation. The microwave power was 800 W and the CH_4 concentration was kept at 1% in the H_2-CH_4 gas mixture. The pressure was kept at 23 torr and the nucleation time for all the samples was 30 minutes.

3.4 Research of Al-based Interlayers on The Adhesion of Diamond Coatings

Six groups of interlayer (Al-AlN, Al-Al_2O_3, Al-Ta, Al_2O_3, Al_2O_3-Ta, Ta) were designed to illustrate the effect of Al-based interlayer on the growth and adhesion of diamond coatings on WC-Co cutting tool materials. The Ta, Al-Ta, Al-Al_2O_3 and Al-AlN interlayered samples were seeded by 1 wt. % diamond suspension for 30 s, while the samples with single Al_2O_3 interlayer and Al_2O_3-Ta were seeded for 15 s to protect the interlayer from spallation. Then all the samples were ultrasonically cleaned in distill water for 10 minutes.

Diamond coatings were deposited using a 2.45 Hz microwave plasma enhanced chemical vapor deposition (MPCVD) system. The microwave power was 800 W in the first 30 min and increased to 1000 W after the initial nucleation and growth. A H_2-CH_4 gas mixture was introduced into the chamber to keep the operation pressure at 23 torr. The composition of CH_4 was kept at 1% for the first 30 minutes as nucleation step and then reduced to 0.75% for diamond growth of 12 hours.

The thickness of all the samples after 12 hours deposition is approximate 1 µm (from 0.9 to 1.1 µm) measured by optical profilometer manufactured by Zygo (Fig. 3-3).

Figure 3-2. Microwave plasma enhanced chemical vapor deposition instrument (from Plasmionique)

3.5 Characterization of Interlayers and Diamond Coatings

The thickness of each interlayer was measured using Zygo NewView 8000 Optical Profilometer (Fig. 3-3). Raman spectroscope (Fig. 3-4, Renishaw 2000, Ar laser with wavelength of 514 nm) and Scanning Electron Microscope (Fig. 3-5, SEM, JSM 840A 10 kV) were used to evaluate the bonding states and microstructure of the deposited diamond coatings, respectively. Grazing Incidence X-ray Diffraction (GIXRD) was conducted at HXMA beamline, Canadian Light Source, to characterize the crystalline structures of the interlayers (Fig. 3-6). Rockwell C indentation testing was carried out with a load of 1470 N to evaluate the adhesion of diamond coatings. Energy Dispersive X-ray spectroscopy (EDS) was used to analyze the composition around the failed interface of the coatings.

Figure 3-3. Zygo NewView 8000 optical profilometer

Figure 3-4. Renishaw 2000 Raman spectroscope

Figure 3-5. JEOL JSM-6010LV SEM

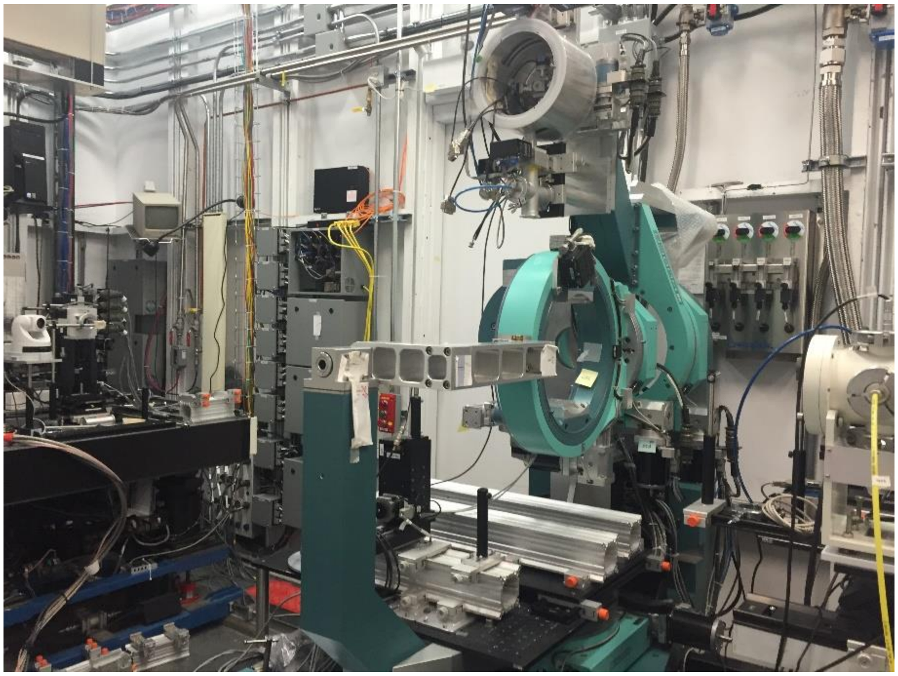

Figure 3-6. Synchrotron based GIXRD, Canadian Light Source

3.6 Research of Tribological Property of Diamond Coatings

The diamond coating deposited on Al-AlN interlayered WC-Co sheet which exhibits the best adhesion property was chosen to compare its tribological property with that of bare WC-Co sheets and the diamond coating deposited on WC-Co sheets pre-etched by Murakami's solution and Caro's acid. The as-polished WC-Co sheets were first immersed in ultrasonic bath of Murakami's solution (10 g $K_3[Fe(CN)_6]$ + 10 g KOH + 100 mL H_2O) for 10 minutes, followed by Caro's acid (3 mL H_2SO_4 (96%) + 88 mL H_2O_2 (30%)) etching for 10 seconds. Then the samples were ultrasonically cleaned in distilled water for 10 minutes.

The etched WC-Co sheets were seeded with 1 wt.% nano-diamond suspension for 30 seconds and then put into 2.45 Hz MPCVD reactor for diamond deposition. The deposition parameters are same with that used to deposit diamond coatings on interlayered samples, as described in Section 3.4.

Tribometer (Fig. 3-7) was employed to conduct the "pin-on-flat" dry tribo-test at room temperature. 440C stainless steel balls and Al_2O_3 balls with diameter of 4 mm were pressed on the coated samples respectively with a vertical load of 5 N. The balls move linearly on the samples reciprocally for 10,000 cycles with the speed of 5 mm/s and the wear track was 2.5 mm. The wear volume of the sheet surfaces was directly measured using the optical profilometer (Fig. 3-3).

Different groups of the test are listed in the table 3-2. The tribo-testing in each group was conducted for two times.

Table 3-2. Groups of Tribo-test

Group No.	Sheet Surface	Ball Counterparts
1	Bare WC-Co	440C stainless steel ball
2	Bare WC-Co	Al_2O_3 ball
3	Diamond coating on WC-Co sheet pre-etched by Murakami's solution and Caro's acid	440C stainless steel ball
4	Diamond coating on WC-Co sheet pre-etched by Murakami's solution and Caro's acid	Al_2O_3 ball
5	Diamond coating on Al-AlN interlayered WC-Co sheet	440C stainless steel ball
6	Diamond coating on Al-AlN interlayered WC-Co sheet	Al_2O_3 ball

Figure 3-7. CETR UMT tribometer

CHAPTER 4
RESULTS AND DISCUSSION

4.1 Effect of Seeding Conditions on Diamond Nucleation

Fig. 4-1 provides the surface morphological images of Al-AlN interlayered WC-Co sheets with different seeding conditions after 30 minutes of diamond deposition. The microwave power and the CH_4 concentration for diamond nucleation was set at 800 W and 1% respectively. Because the interlayer is very easy to be scratched by diamond powders, the seeding time for all the samples is 30 seconds. The black particles in the images might be pinholes in the interlayer while the white particles are the diamond nuclei. It can be observed that the nucleation density of the samples ultrasonically scratched with nano-diamond powders (Fig. 4-1 b, d, f) is higher than that of those scratched with micro-diamond powders (Fig. 4-1 a, c, e), whereas the nuclei formed on the micro-diamond scratched samples are generally larger than that formed on nano-diamond scratched samples. This is in agreement with research findings of Itoh [101] that the nucleation density increases with decreasing grain size of diamond powders used for ultrasonic scratching prior to diamond deposition. It is explained by the fact that the number of diamond powders increases with the decreasing powder size for a given weight of diamond powders. Therefore the possibility of diamond powders colliding with the sample surfaces increases, resulting in more defects on the surface and more powders imbedded into the samples.

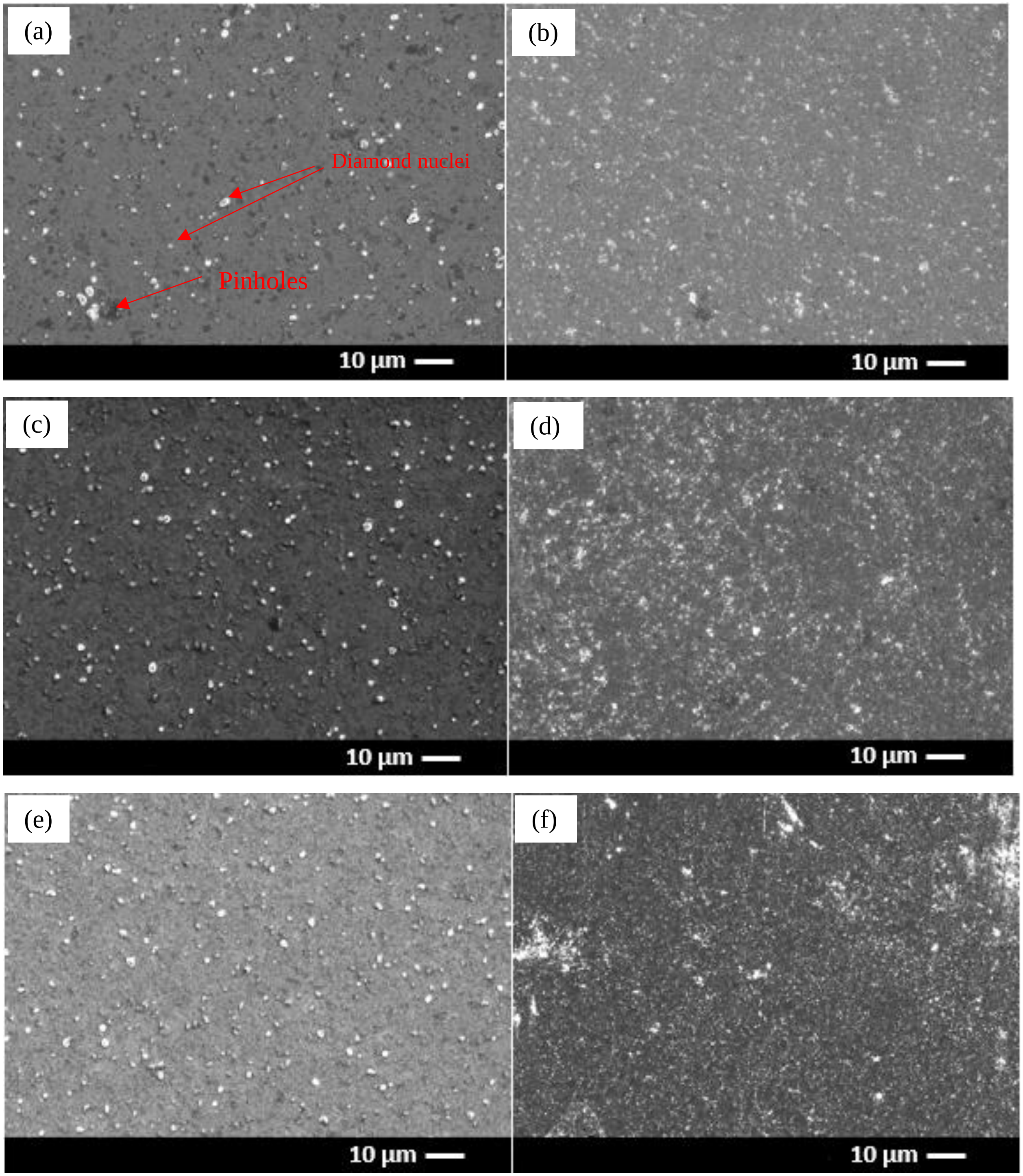

Figure 4-1. Surface morphology of diamond nucleation on Al-AlN interlayered WC-Co sheets seeded by (a) 0.5 wt.% micro-diamond, (b) 0.5 wt.% nano-diamond, (c) 1 wt.% micro-diamond, (d) 1 wt.% nano-diamond, (e) 3 wt.% micro-diamond, (f) 3 wt.% nano-diamond suspensions

On the other hand, it can be found that the nucleation density increases with the concentration of diamond powders in the suspensions. The nucleation density of the sample seeded by 3 wt.%

diamond suspension are obviously higher than that seeded by 0.5 wt.% diamond suspension due to high collision frequency. Additionally, continuous diamond coatings can be found in some regions of the samples seeded by 1 wt.% or 3 wt.% nano-diamond powders after 30 minutes of diamond deposition, as shown in Fig. 4-2. No continuous coatings can be found in micro-diamond seeded samples. On the surface of the sample seeded by 1 wt.% micro-diamond, continuous coating only forms in limited area along the defects and scratches even after 12 hours deposition, shown in Fig. 4-3.

Therefore, nano-diamond powders (grain size averaged around 3-4 nm) are more suitable than micro-diamond powders (grain size around 1 μm) for diamond seeding on Al-AlN interlayered WC-Co sheets. Since the continuous diamond coatings can be found on the sample surfaces seeded by both 1 wt.% and 3 wt.% nano-diamond suspensions after 30 minutes nucleation, the 1 wt.% nano-diamond suspension was employed in further research to pre-seed the Al-based samples.

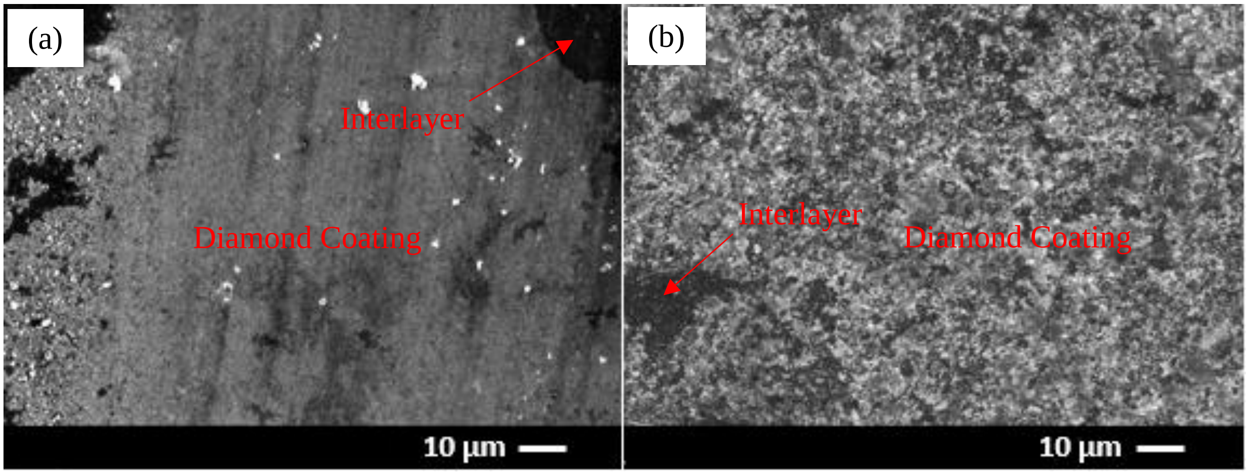

Figure 4-2. Continuous diamond coatings formed in some areas on Al-AlN interlayered WC-Co sheets seeded by (a) 1 wt.% nano-diamond suspension and (b) 3 wt.% micro-diamond suspension after 30 minutes nucleation

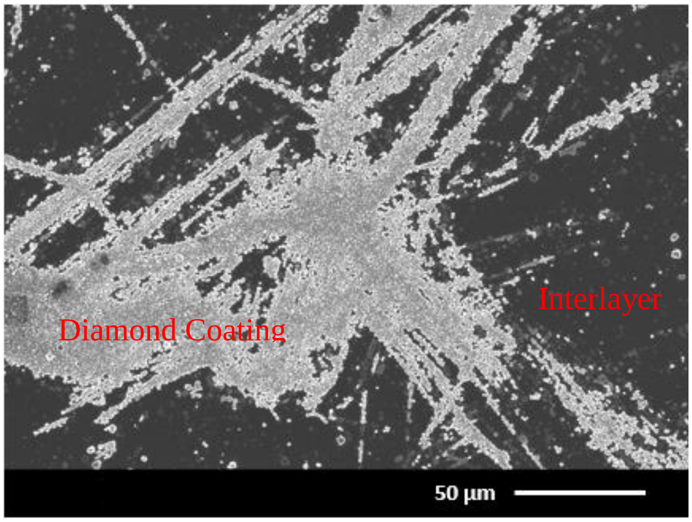

Figure 4-3. Surface morphology of the diamond coating on Al-AlN interlayered sample seeded with 1 wt.% micro-diamond suspension after 12 hours deposition

4.2 CVD Diamond Coating on WC-Co Substrate with Al-based Interlayer

4.2.1 Characterization of Interlayers

In order to investigate the effect of Al interlayer in suppressing the diffusion of Co and optimize the sublayer on top of Al, six groups of interlayer including Al-Al_2O_3, Al-AlN, Al-Ta, Al_2O_3, Al_2O_3-Ta and Ta were designed. Fig. 4-4 shows the Grazing Incidence X-ray Diffraction patterns of Al-Al_2O_3 and Al-AlN interlayers before diamond deposition. The energy of the employed X-ray is 17,998 eV. At a low incident angle of 0.05°, the peaks of Al (220), (311), (222) and (400) are clearly detected in both Al-Al_2O_3 and Al-AlN interlayered samples. In Al-Al_2O_3 interlayered sample, a peak assigned to ϒ-Al_2O_3 is observed. This is in agreement with Edlmayr's research [126] that only one peak of ϒ-Al_2O_3 can be detected in XRD pattern for Al_2O_3 deposited by sputtering at room temperature. One noticeable fact is that this peak can also be observed in Al-AlN interlayered samples, which supports our previous conclusion that an ultrathin Al layer can be oxidized in a high vacuum environment [125]. Besides Al and Al_2O_3 peaks, two AlN peaks, (110) and (211), are found in Al-AlN interlayered samples, indicating the formation of AlN on the top of Al sublayer. When the incident angle increased to 1°, the intensity ratio of interlayers to WC substrate decreases since the thickness of interlayer is as thin as approximately 200 nm, less than the X-ray penetration depth.

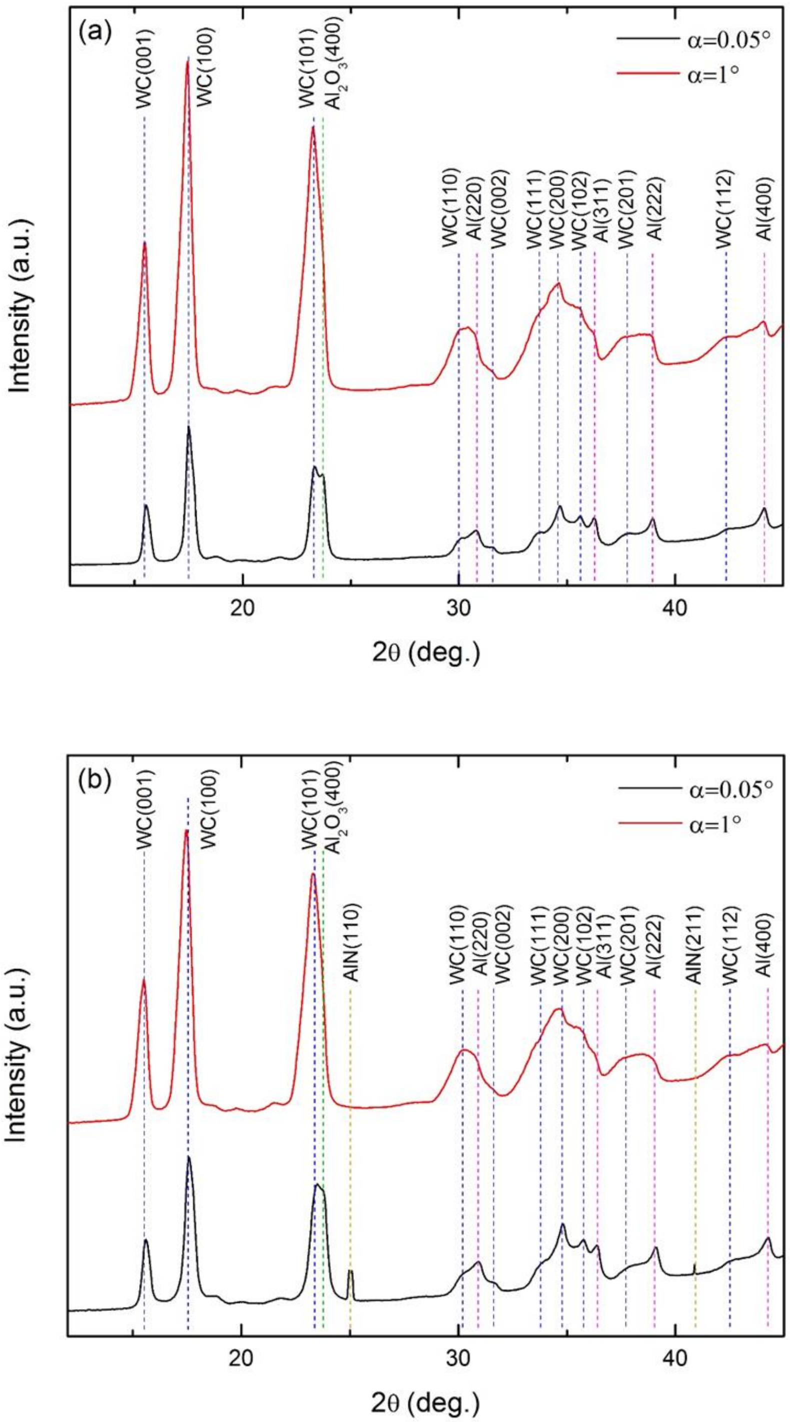

Figure 4-4. GIXRD patterns of interlayer (a) Al-Al_2O_3 and (b) Al-AlN

4.2.2 Characterization of Diamond Coatings

Fig. 4-5 (a-d) shows the surface morphology of the diamond coatings deposited on Al-Al_2O_3, Al-AlN, Al-Ta and Al_2O_3 interlayered WC-Co sheets. After 12 hours deposition, a continuous diamond coating was synthesized on all the samples except for the one with a single Ta interlayer. The average grain size of the diamond coating with a single Al_2O_3 interlayer is approximate 1.25 µm, obviously greater than those on the other three samples coated with an additional Al sublayer. This may be caused by the shorter diamond seeding time (10 s vs 30 s). A long pretreatment period has been observed to damage the interlayer as the solid Al_2O_3 layer has relatively low adhesion to the WC-Co substrate due to lack of strong interfacial bonding. The average grain size of diamond on Al-Al_2O_3, Al-AlN and Al-Ta interlayered samples is very similar at a submicron scale. The diamond grown on Al-Ta interlayer shows the smallest average grain size of approximately 0.69 µm, which is probably attributed to the fact that metal Ta has strong carbide forming ability and thus facilitates the nucleation of diamond. The diamond grown on Al-Al_2O_3 and Al-AlN interlayers has a similar average grain size of approximately 0.88 µm. But for Al_2O_3-Ta and single Ta interlayered samples, the diamond coatings have very poor adhesion to the substrate and the coatings peel off spontaneously after cooling down from deposition, as shown in Fig.4-5 (e and f).

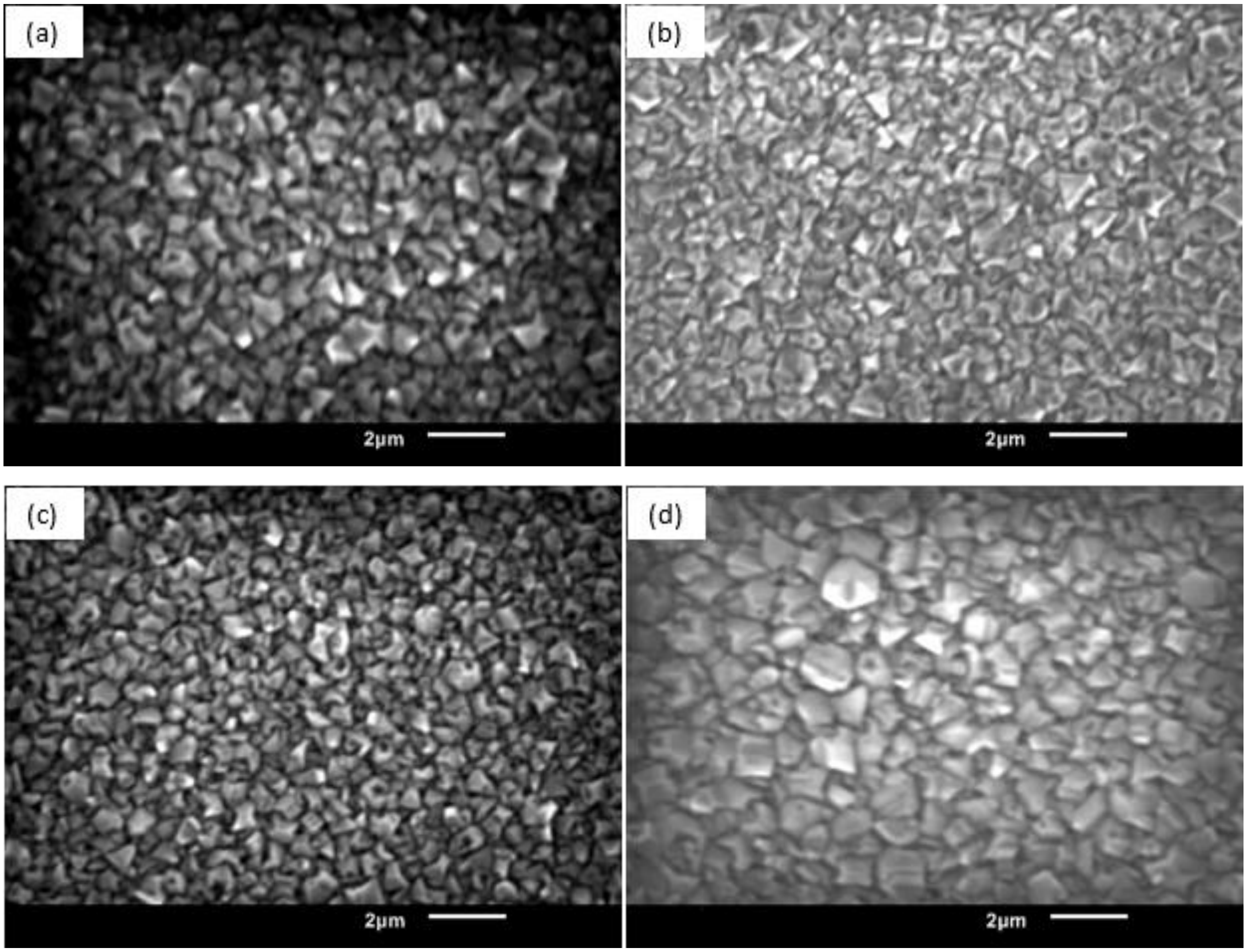

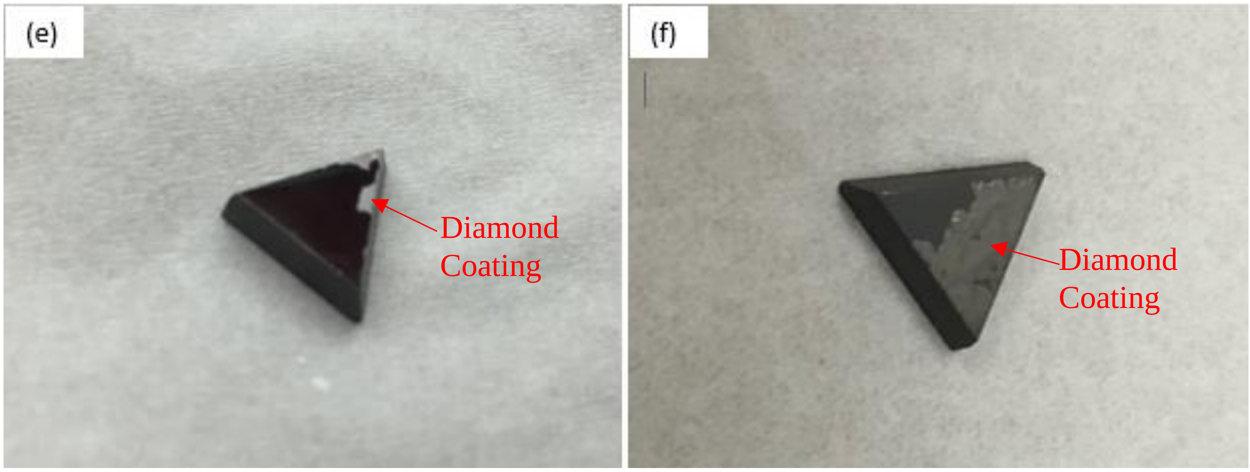

Figure 4-5. Surface morphology images of diamond coating grown on (a) Al-Al_2O_3, (b) Al-AlN, (c) Al-Ta, (d) Al_2O_3, (e) Al_2O_3-Ta and (f) Ta interlayered WC-Co substrate

The Raman spectra of diamond coatings deposited with various interlayers are presented in Fig. 4-6. In the spectra of diamond coating on Al-Al_2O_3 and Al-AlN interlayered samples, the peaks of diamond are located at 1335 cm^{-1}. The upward shifting of the diamond peak in comparison with that of nature diamond at 1332 cm^{-1} indicates the existence of compressive stress in the coating due to the mismatch of thermal expansion coefficients of diamond coating with the substrate [80], which suggests that the coating is continuous and adheres to the substrate. In the spectrum of diamond deposited on single Al_2O_3 interlayered samples, the peak of diamond shifted to 1336 cm^{-1}, indicating that the compressive stress is higher than those in Al-AlN and Al-Al_2O_3 interlayered samples. Considering the largest size of diamond grain observed in SEM images (Fig. 4-5d), the higher stress is possibly caused by the nearby grain squeezing during the growth of diamond. The diamond peak of the coating on Al-Ta interlayered samples shifts even higher to 1336.6 cm^{-1}, implying even higher compressive stress. In addition, there is a strong peak located around 1370 cm^{-1} seen in the spectrum of diamond deposited on single Al_2O_3 interlayered samples. This peak might be attributed to the scattering of graphitic carbon, indicating that a single Al_2O_3 interlayer is not sufficient to suppress the Co diffusion into the coating to catalyze graphitic carbon formation. There is another weak broad peak around 1530 cm^{-1}, corresponding to amorphous carbon [77], appearing in both the spectra of single Al_2O_3 coated and Al-AlN coated samples. Weak broad peaks around 1150 cm^{-1} and 1440 cm^{-1} are also observed in the spectra of Al_2O_3, Al-Al_2O_3 and, Al_2O_3-Ta and Al-AlN interlayered samples, which are related to the formation of nanodiamond and probably attributed to the scattering of trans-polyacetylene [77, 127]. The Raman spectra of the coatings on single Ta interlayered and Al_2O_3-Ta interlayered samples (Fig. 4-6 e and g) show a diamond peak at 1332 cm^{-1}, suggesting the stress is completely released due to the spallation of the coating. On the exposed substrate area where coating has peeled off, two broad peaks located at 1345 cm^{-1} and 1605 cm^{-1} are observed (Fig. 4-6 f and h), revealing the formation of a graphitic intermediate layer between the diamond coating and the substrate.

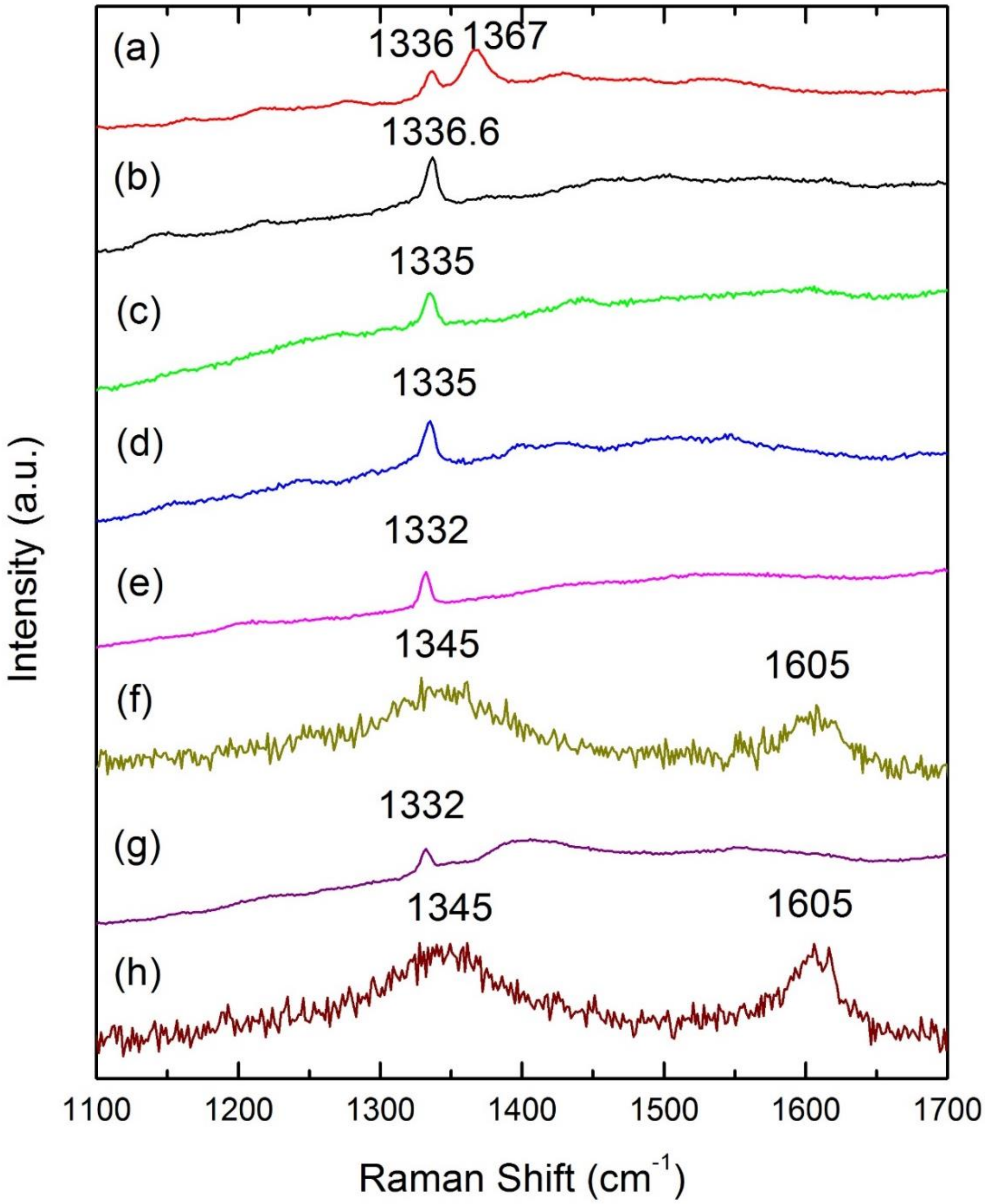

Figure 4-6. Raman spectra of diamond coating grown on (a) Al_2O_3, (b) Al-Ta, (c) Al-Al_2O_3, (d) Al-AlN, (e) Ta and (g) Al_2O_3-Ta interlayered WC-Co substrate, and (f) graphite on Ta interlayered and (h) Al_2O_3-Ta interlayered WC-Co substrate

4.2.3 The role of Al

The data shown above indicates the positive effect of Al layer in restricting the formation of graphitic carbon. The Raman spectrum of samples coated with Al sublayer shows one primary peak located at around 1335 cm^{-1} (Fig. 4-6a), implying the formation of high purity diamond in the coating. Other peaks at approximately 1530 cm^{-1} and 1440 cm^{-1} are ignorable compared with intensity of diamond peak. As shown in Fig. 4-6b, a single Ta interlayer is not sufficient to prevent the formation of graphitic carbon at the interface, whereas an Al-Ta double interlayer can. Because the graphitic carbon is usually formed due to the catalytic effect of Co, indicating that the presence of Al sublayer can efficiently suppress the diffusion of Co and isolate the carbonaceous gas species from contacting with Co in the substrate. Our group's previous work has proposed that the Al layer could be easily oxidized to aluminum oxide layer and such formed aluminum oxide layer is dense and able to block the diffusion of Co and carbon [27, 125]. Whereas the diamond coating formed on the single Al_2O_3 interlayered WC-Co substrate consists of graphitic carbon with a Raman peak around 1370 cm^{-1} (Fig. 4-6a), different from the diamond grown on single Al interlayered substrate [123], which consists of mainly diamond. In addition, the diamond coating deposited on Al_2O_3-Ta interlayered substrate shows the same feature with that of the single Ta interlayered sample in that the diamond coatings were delaminated immediately after CVD (Fig. 4-5 e and f). And the Raman spectrum (Fig. 4-6h) demonstrates that graphite was generated below diamond coating, which suggests that the Al_2O_3 layer formed by reactive sputtering is not effective in suppressing the diffusion of Co.

The different ability of metallic Al layer and Al_2O_3 layer in suppressing the diffusion of Co could be explained from two aspects. Firstly, the melting temperature of Al is as low as 660 °C. It is believed that the Al layer melts during diamond deposition using 1000 W microwave power. At this case, the substrate temperature should be well above the melting point of Al [28]. But Al_2O_3 layer has much higher melting point than the diamond deposition temperature which is usually not higher than 900 °C. Therefore Al_2O_3 layer would keep its solid state during diamond deposition. As we know, a thin layer of Al_2O_3 formed by reactive sputtering at low temperature should contain pinholes and other defects for Co diffusion, whereas the melted Al layer has much higher mobility than solid and would react with O_2 to form dense oxide layer before diamond nucleation. Furthermore, the melted Al might diffuse into substrate to form Al-Co alloy to reduce the catalytic effect of Co for promoting graphitic carbon formation [18], where Al donates electrons to Co and changes its 3d electronic structure. In addition, the formation of Al-Co metallic bond at the interface would improve the adhesion of Al interlayer to WC-Co substrate.

4.2.4 Adhesion measurement and analysis

Adhesion tests were conducted on Al-Al_2O_3, Al-AlN and Al-Ta interlayered samples by means of Rockwell C indentation testing. Fig. 4-7 shows the surface morphological features of diamond coatings after indentation tests with a load of 1470 N. Both secondary electron images (SEI) (Fig. 4-7b, d, f) and backscattered electron images (BEI) (Fig. 4-7a, c, e) are provided to illustrate the surface states after indentation tests. For Al-Al_2O_3 interlayered samples, cracking of both diamond coating and interlayer is observed around the imprint area and local delamination of diamond coating appears surrounding the imprint area as shown in Fig. 4-7b. As the contrast in BEI images is primarily from the atomic number difference, brighter area in the BEI image shown in Fig. 4-7a indicates delaminated area, suggesting failure might occur at both the diamond-interlayer and interlayer-substrate interfaces. The strong Co peak and low Al peak EDS spectrum taken from the white area (Fig. 4-8a) suggests that the substrate surface is exposed and both the diamond coating and part of the interlayer is probably delaminated. For diamond coatings on Al-AlN interlayered samples, as shown in Fig. 4-7c and d, only a few cracks are observed around the imprint. The EDS spectrum (Fig. 4-8b) collected from the cracked area demonstrates the crack might occur and extend into the interlayer, as noticeable Co can be detected. Serious delamination of diamond coating is found in Al-Ta interlayered samples (Fig. 4-7e, f). The delamination area is almost double that in Al-Al_2O_3 interlayered samples. Nonetheless, the BEI (Fig. 4-7e) image shows the delamination only occurs at the diamond-interlayer interface because the Co and Al peaks in the EDS spectrum (Fig. 4-8c) of the delamination area are very weak. Instead, a high Ta peak is observed, indicating that Ta adheres well to WC-Co substrate.

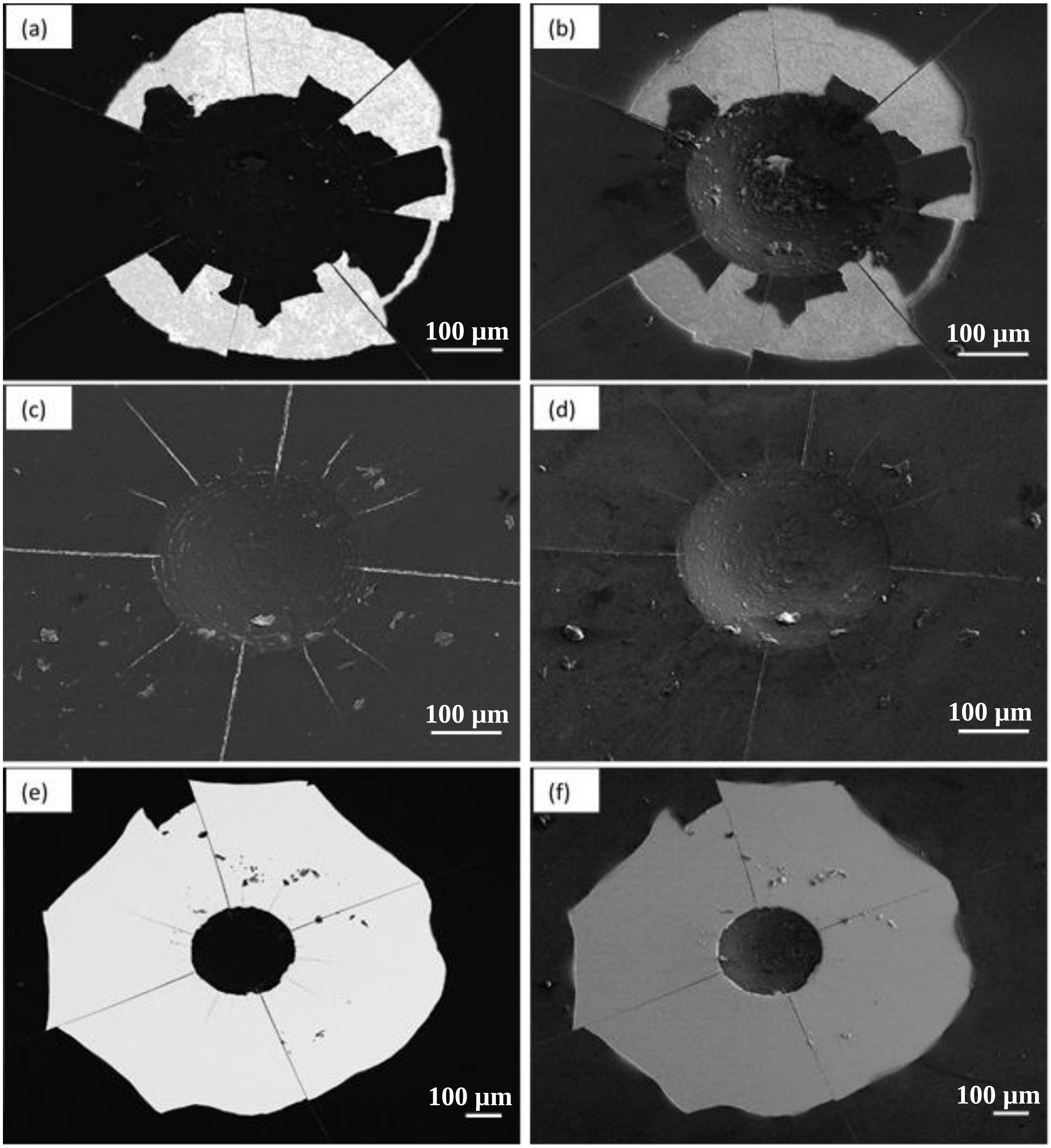

Figure 4- 7. SEM images (BEI) of imprint of diamond coating on (a) Al-Al_2O_3, (c) Al-AlN, (e) Al-Ta interlayered WC-Co substrate, and SEI image of imprint of diamond coating on (b) Al-Al_2O_3, (d) Al-AlN, (f) Al-Ta interlayered WC-Co substrate

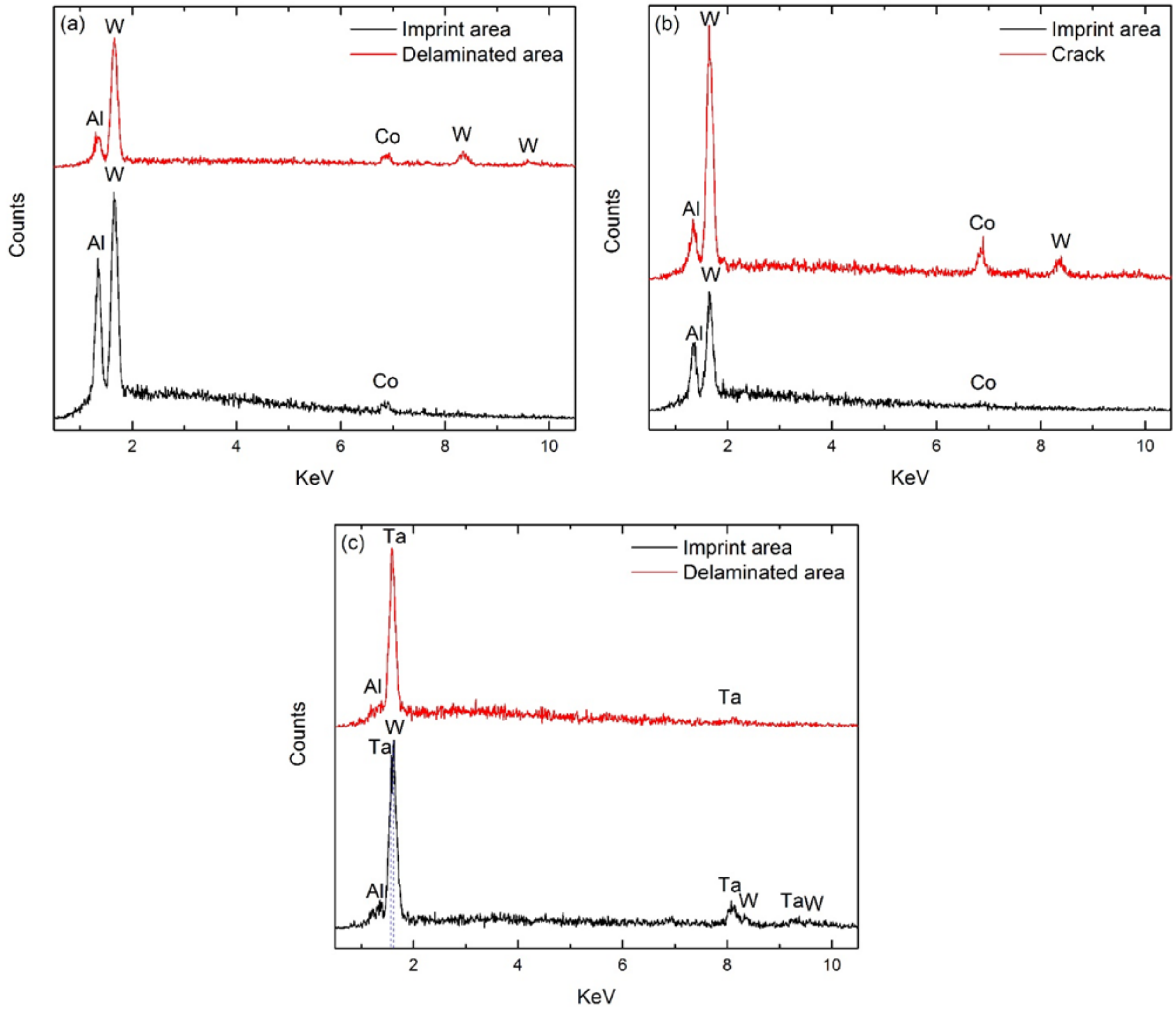

Figure 4-8. EDS spectra of imprint on (a) Al-Al_2O_3, (b) Al-AlN, (c) Al-Ta interlayered WC-Co substrate

The poor adhesion between the Ta interlayer and the diamond coating is probably attributed to the high thermal stress accumulated at the diamond-Ta interface. This result is in consistent with the Raman results (Fig. 4-6a), where diamond peak shows the largest shift to 1336.6 cm^{-1}. Based on Ager and Drory's equation [80], the thermal stress inside the diamond coatings is compressive stress with a value of 2.6 GPa for Al-Ta interlayered samples and 1.7 GPa for Al-Al_2O_3 and Al-AlN interlayered samples. Considering the higher diamond nucleation density on Ta than on Al_2O_3 or AlN, it is reasonable to attribute its poorer adhesion to the higher thermal stress.

Even though the Raman spectra reveal that the diamond coatings grown on Al-Al_2O_3 or Al-AlN interlayered samples have a similar compressive stress (Fig. 4-6a), the adhesion of diamond coating on Al-Al_2O_3 interlayer is much worse than that on Al-AlN interlayer (Fig.4-7a, b). The reason is that diamond usually has a high nucleation density on AlN [128, 129], which can be attributed to the formation of an intermediate aluminum carbide sublayer on the AlN surface during the initial deposition stage in hydrogen and methane plasma. Although the diamond nucleation density on aluminum oxide is still not thoroughly investigated, the better adhesion of diamond coating to AlN suggests possible higher diamond nucleation density on AlN.

4.3 Tribological property of diamond coated WC-Co sheets

4.3.1 Surface Morphology of Diamond Coatings

Tribological property of the diamond coatings deposited on Al-AlN interlayered WC-Co substrates is compared with the bare WC-Co sheets and the diamond coatings deposited on WC-Co sheets pre-etched by Murakami's solution and Caro's acid. Fig. 4-9 is the surface morphological images of diamond coatings deposited on WC-Co sheets which were pre-etched by Murakami's solution and Caro's acid. Compared with the diamond coatings deposited on the interlayered WC-Co substrates (Fig. 4-5), many diamond clusters can be observed on the surface pre-etched WC-Co substrates, as shown in Fig. 4-9a. This is probably caused by the increased roughness of WC-Co substrate after Murakami's solution etching since the Murakami's reagent is able to attack WC and coarsen the grains. In the magnified image (Fig. 4-9b), cauliflower structure diamond clusters, which consists of nanocrystalline diamond (NCD) grains, are found mixed with the polycrystalline diamond. Cauliflower structure diamond usually contains higher sp^2 bond [130], as shown in the Raman spectrum (Fig. 4-10). The peak at 1334 cm^{-1} is attributed to diamond crystals and the peak at 1590 cm^{-1} indicates the presence of graphitic phase. Compared with the Raman spectrum of diamond coating deposited on Al-AlN interlayered WC-Co sheet (Fig. 4-6d), the obvious high intensity of sp^2 peak implies more graphitic phase in cauliflower structure diamond clusters. However the Raman scattering intensity of amorphous carbon or graphite is approximately 50 times higher than diamond, so the diamond phase is still dominant in the diamond coatings [131]. The peak at 1411 cm^{-1} is probably attributed to the sp^2 bonded carbon existing between nanocrystalline diamond grains [132].

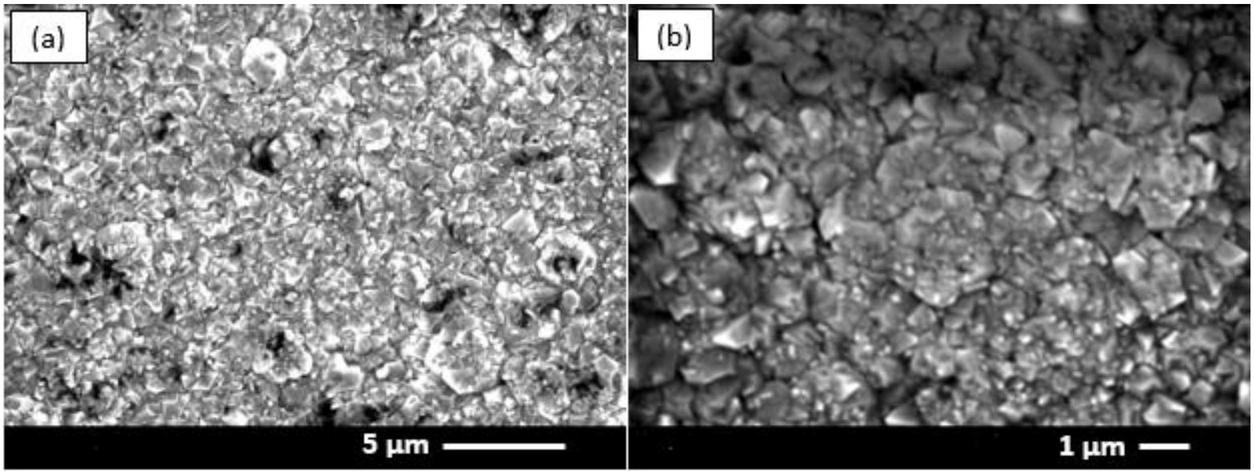

Figure 4-9. Surface morphological image of (a) diamond coating deposited on WC-Co sheet pre-etched by Murakami's solution and Caro's acid and (b) magnified image

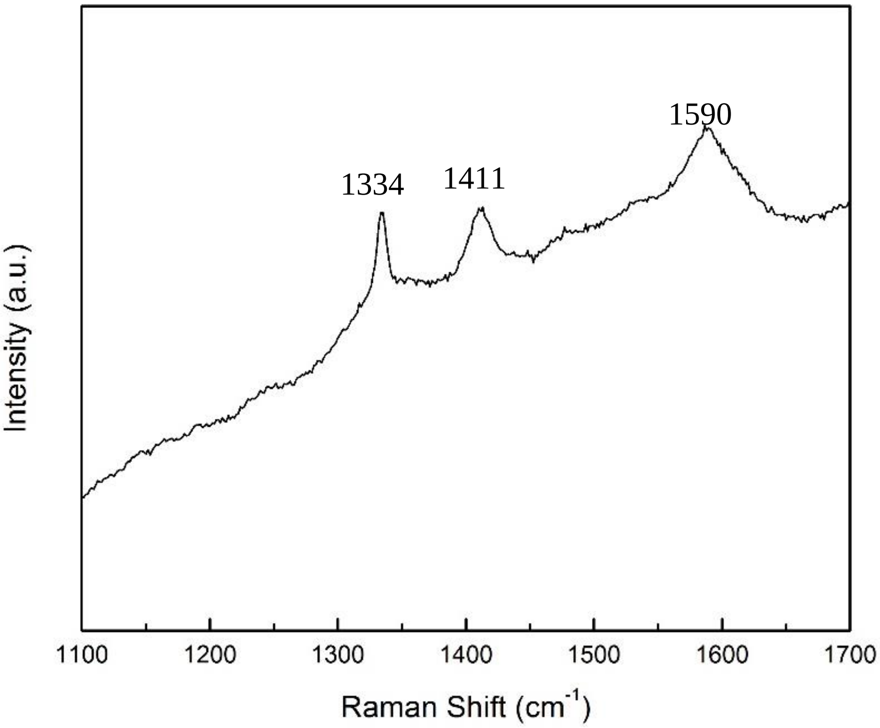

Figure 4-10. Raman spectrum of diamond coatings grown on WC-Co sheets pre-etched by Murakami's solution and Caro's acid

4.3.2 Coefficient of Friction

The coefficient of friction (COF) of each sample at stable reciprocating frictional motion are presented in Fig. 4-11. The orange bar indicates the COF obtained using 440C stainless steel ball, while the red bar is the COF obtained by using alumina ball.

The COF is around 0.69 in the tribo-test group 1 where steel ball rubbing against the bare WC-Co sheet, much higher than that in other tribo-test groups. This may be explained by the interaction of dangling bonds between Co from the carbide sheet and Fe from the steel ball [99]. The COF drops to approximate 0.33 when alumina ball is applied in the tribo-test because of reduced interaction between the ball and the substrate.

When the WC-Co sheets are coated with the diamond, the COF drops regardless of whether steel or alumina ball was used. As shown in the Fig. 4-11, the COF of the samples rubbed by steel ball is always slightly higher than that rubbed by alumina ball. This is probably caused by the diffusion of carbon from the diamond coatings into the steel balls during the tribo-test resulting in the formation of carbide on the steel ball surface. Then the interaction of C dangling bonds from the diamond coating and steel ball contributes to the higher frictional force and hence increase the COF. In addition, the COF of diamond coatings deposited on chemical etched WC-Co sheets are slightly less than that of diamond coatings deposited on Al-AlN interlayered WC-Co sheets, regardless of whether steel or alumina ball was used. Even though the surface roughness of diamond coatings on chemical etched WC-Co sheets (RMS 290 μm) is higher than that on Al-AlN interlayered sample (RMS 76 μm) due to the presence of diamond clusters on the surface, the higher graphitic phase in cauliflower structure diamond is believed to reduce the frictional force due to the lamellar structure of graphite [130].

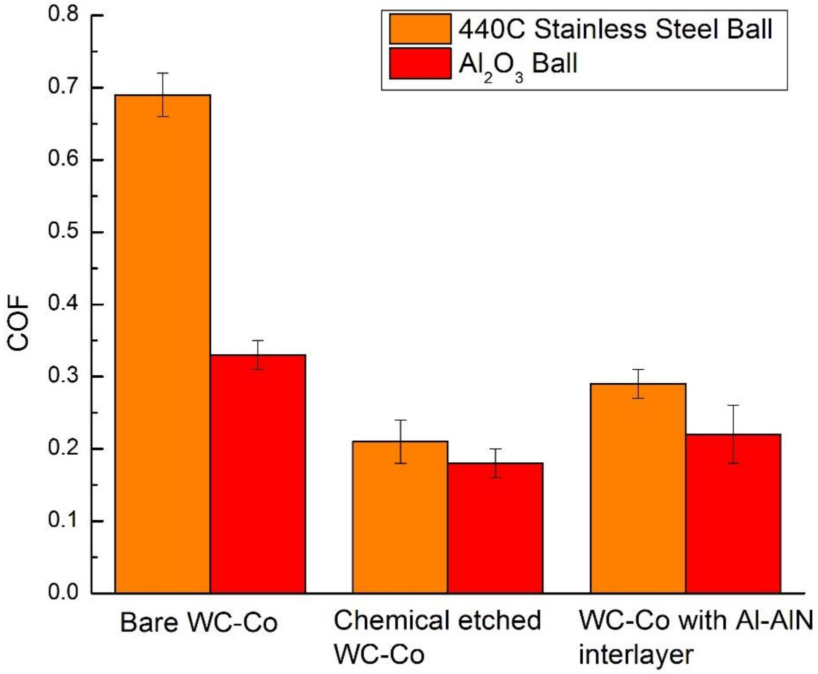

Figure 4-11. Coefficient of Friction of samples rubbing against steel ball and alumina ball

4.3.3 Wear of Sheet Surface and Ball

Fig. 4-12 and Fig. 4-13 show the wear scars on the sample surfaces and the corresponding rubbing balls respectively. Group 1 is the bare WC-Co/steel ball, Group 2 is the bare WC-Co/alumina ball, Group 3 is the diamond coating on chemical etched WC-Co/steel ball, Group 4 is the diamond coating on chemical etched WC-Co/alumina ball, Group 5 is the diamond coating on Al-AlN interlayered WC-Co/steel ball, Group 6 is the diamond coating on Al-AlN interlayered WC-Co/alumina ball. For all the samples coated with diamond, no delamination was found after tribo-test, implying the good adhesion of diamond coatings on the WC-Co sheets regardless of chemical etching pretreatment or interlayer application.

As shown in Fig. 4-12, wear scars of diamond coated samples have broader width than that of bare WC-Co sheets, regardless of using steel ball or alumina ball. Additionally, the wear scar width of diamond coatings are very close with the wear scar width of the ball counterparts as shown in Fig. 4-13. This can be explained by the fact that the diamond coating has much higher hardness than the steel or alumina so that the balls are more likely to be worn out. Therefore, the wear scar width of the diamond coatings reflect the wear of the ball counterparts. With respect to the bare WC-Co (Group 1 and 2), the wear width either on the sheet surface or on the ball is smaller than that on the diamond coated samples. The wear scar widths of the WC-Co sheet and the alumina ball in Group 2 are both smaller than that of Group 1. Considering the much lower COF of WC-Co/alumina ball contact (Group 2) than WC-Co/steel ball contact (Group 1), it is reasonable that the WC-Co sheet and the alumina ball in Group 2 are less worn out.

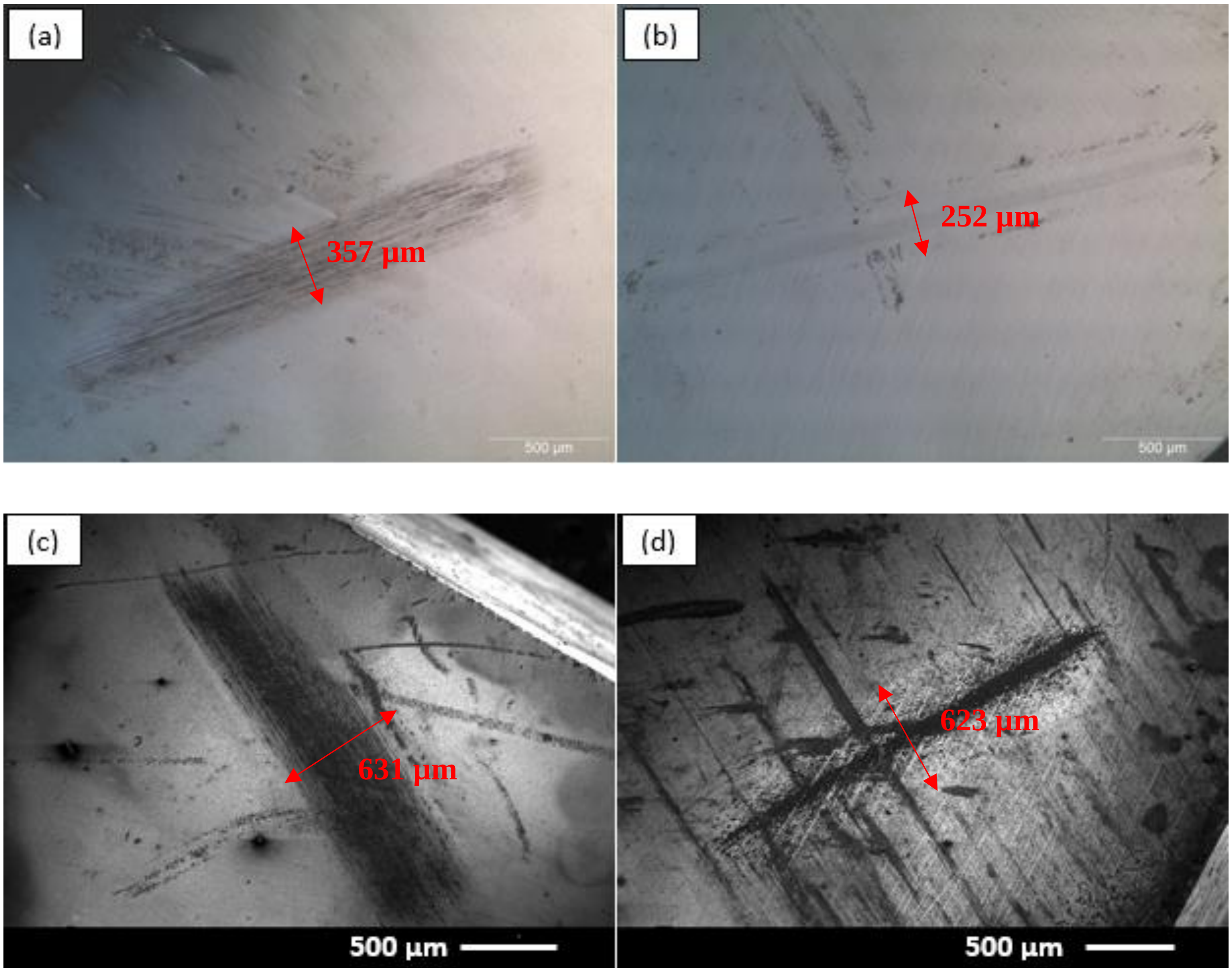

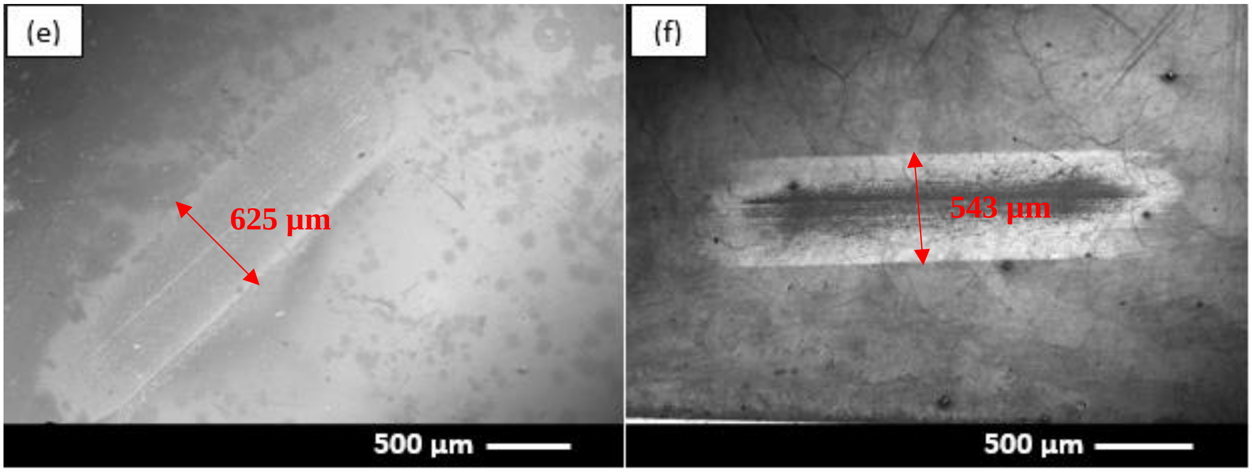

Figure 4-12. Worn surfaces of bare WC-Co surface in (a) Group 1, (b) Group 2 and diamond coatings in (c) Group 3, (d) Group 4, (e) Group 5 and (f) Group 6

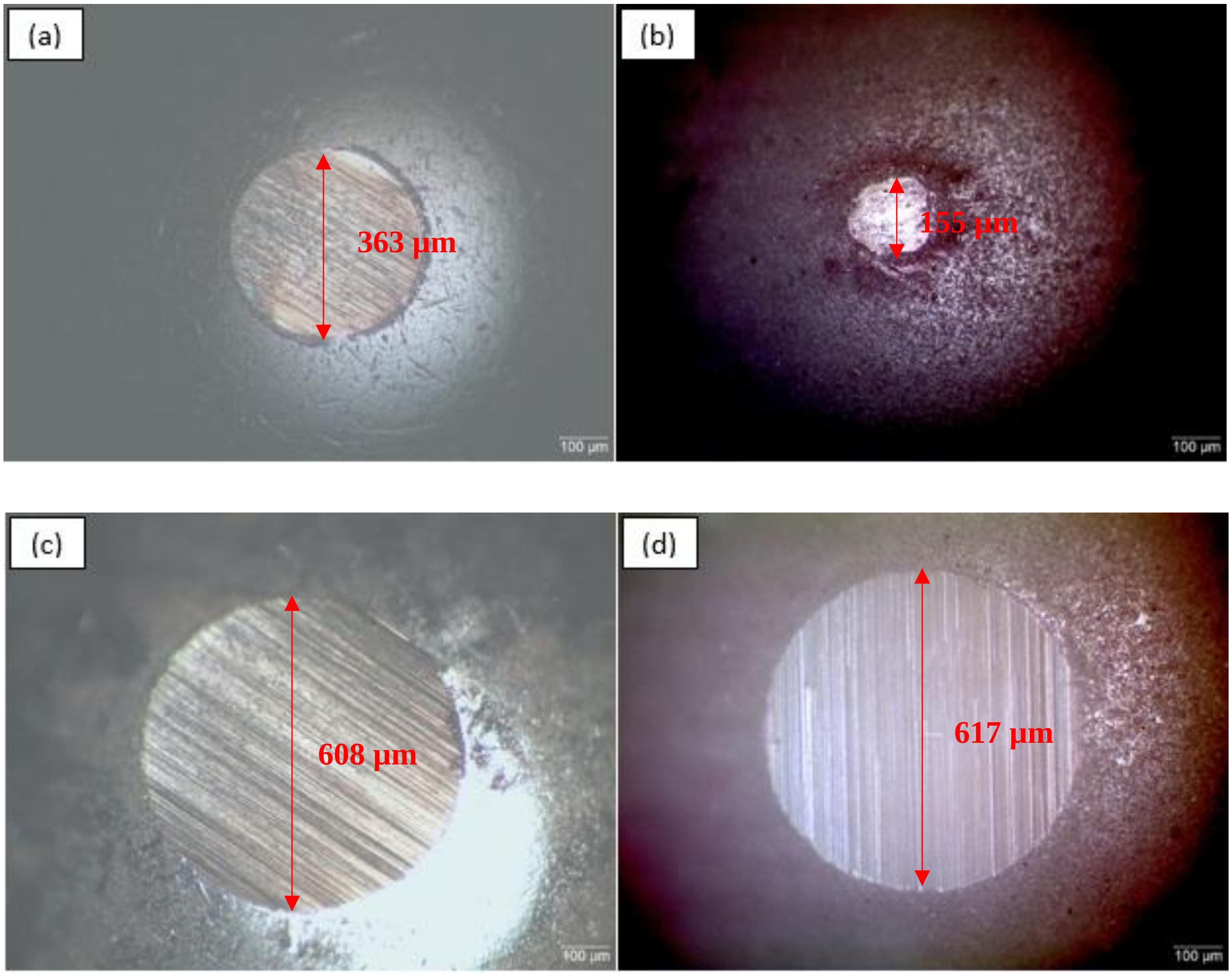

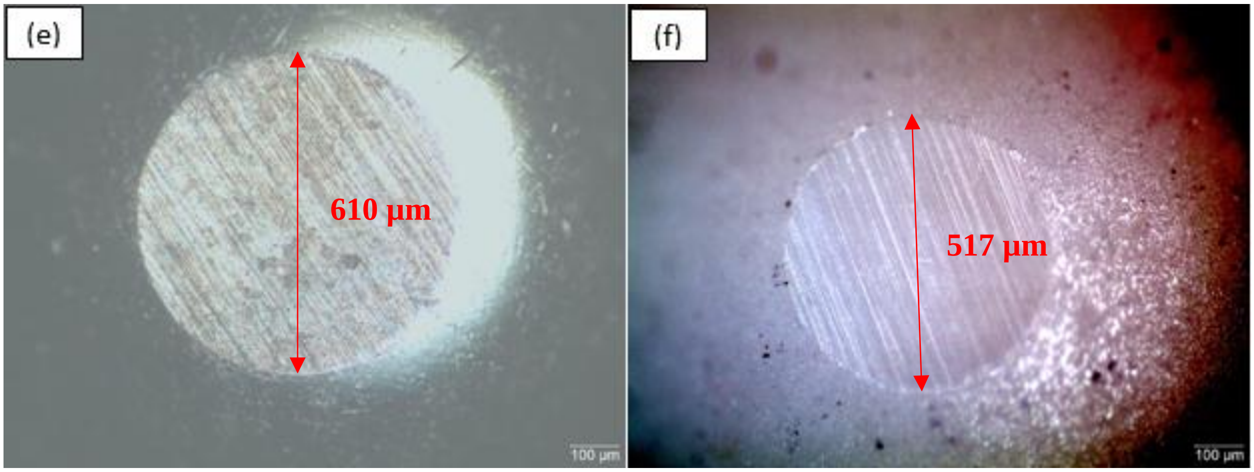

Figure 4-13. Wear scars of the ball counterpart in (a) Group 1, (b) Group 2, (c) Group 3, (d) Group 4, (e) Group 5, and (f) Group 6

The wear rate of the sheet surfaces and the ball counterparts are shown in the Fig. 4-14 and Fig. 4-15 respectively. The wear volume of the sheet surfaces can be directly measured from the optical profilometer so that the wear rate can be calculated based on the equation 4.1[130]:

$$K = \frac{V}{WL} \tag{4.1}$$

The wear rate of ball counterparts can be calculated by the equation 4.2 [133]:

$$K = \frac{\pi d^4}{64rWL} \tag{4.2}$$

Where V is the wear volume, W is the normal force, L is the sliding distance of the ball, d is the diameter of the near circular wear scar on the ball, r is the radius of the ball.

The bare WC-Co sheets generally have higher wear rate than the diamond coated samples, suggesting diamond coatings can successfully protect the WC-Co sheets and improve their wear resistance. The highest wear rate was obtained for bare WC-Co/steel ball contact, reaching to approximate 6.9×10^{-7} $mm^3N^{-1}m^{-1}$. This result is consistent with its COF value that is also highest among all the test groups (Fig. 4-11). With respect to diamond coated samples, the wear rate of diamond coatings on chemical pre-etched samples (Group 3 and 4) is slightly higher than that on Al-AlN interlayered samples (Group 5 and Group 6) in spite of whether steel or alumina ball is applied in the tribo-tests. This is not in agreement with the low COF in Group 3 and 4 as shown in the Fig. 4-11. This may be caused by the high roughness of the diamond coatings in Group 3 and 4 due to the diamond clusters on the surface. The low COF is obtained at stable frictional motion of the steel ball against the diamond surface when the diamond clusters have been ground relatively flat. The higher wear volume is calculated when the rough surface reference is taken into account. The relatively low wear rate of the diamond coating deposited on Al-AlN interlayered sample suggests that not only the Al-AlN interlayer can enhance the adhesion of diamond coatings on WC-Co sheets but also the diamond coatings deposited on Al-AlN interlayer have enhanced the wear resistance. The lowest wear rate (1.75×10^{-7} $mm^3N^{-1}m^{-1}$) was observed in Group 6 where diamond coating was deposited on Al-AlN interlayered sample and rubbed against alumina ball.

The wear rate of the balls as shown in Fig. 4-15 demonstrates that the balls were seriously worn when rubbing against the diamond coatings. The wear rate of the steel balls rubbing against diamond coatings (Group 3 and 5) is found much higher than that rubbing against bare WC-Co sheet (Group 1). When rubbing against diamond coatings (Group 4 and 6), the wear rate of the alumina balls is even two order of magnitude higher than bare WC-Co sheets (Group 2). Therefore it is much more efficient for diamond coated carbide tools to cut alumina materials.

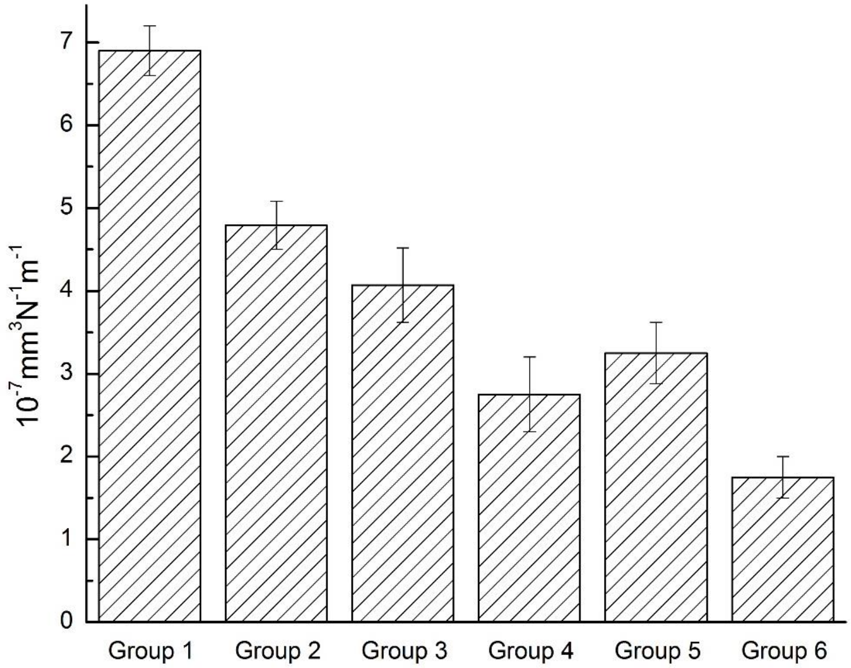

Figure 4-14. Wear rate of the sheet surfaces

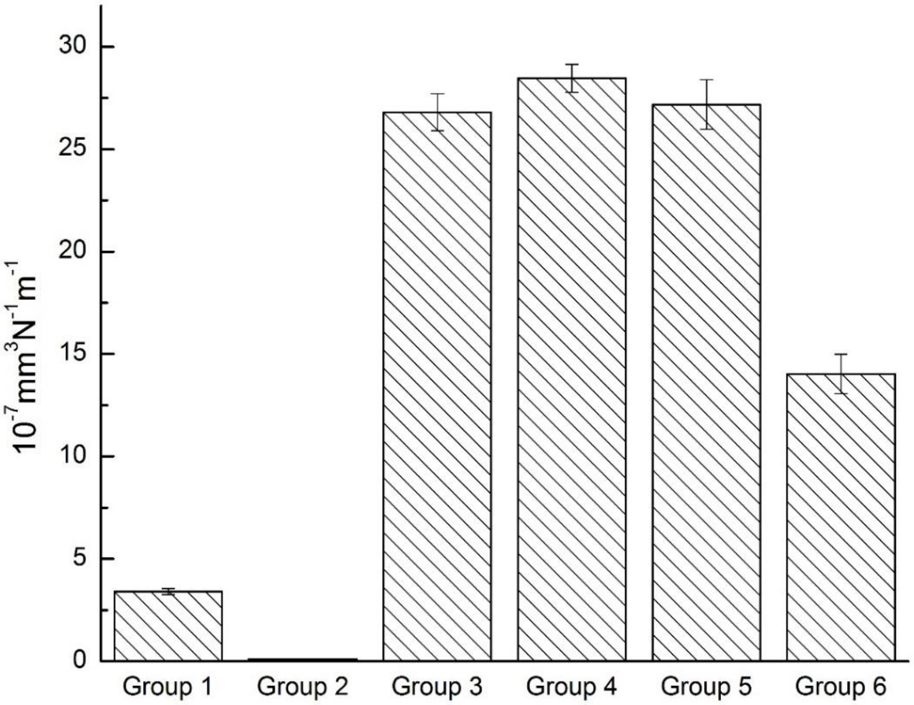

Figure 4-15. Wear rate of the balls

Chapter 5

SUMMARY, CONCLUSIONS AND FUTURE WORK

5.1 Summary and Conclusions

In this work, diamond coatings were deposited on WC-Co sheets by MPCVD with Al-based materials as interlayers. The interlayers were deposited on the substrates using magnetron sputtering. The effect of seeding of different sized diamond particles on the diamond nucleation was also investigated. The tribological properties of the diamond coatings deposited on Al-AlN interlayered WC-Co substrates were compared with those of bare WC-Co sheets and the diamond coatings deposited on the WC-Co sheets that were pre-etched by Murakami's solution and Caro's acid. The following conclusions can be drawn from research findings:

1. Seeding by nano-diamond powders with grain size of 3-4 nm on Al-AlN interlayered WC-Co sheets are more efficient in enhancing the nucleation density than micro-diamond powders with grain size of approximate 1 µm if the seeding time are kept around 30 seconds.

2. After 30 minutes of MPCVD with the power of 800W and the CH_4 concentration of 1 %, continuous diamond coatings can be observed in some areas of the Al-AlN interlayered WC-Co substrates which were seeded by the diamond suspensions containing higher than 1 wt.% nano-diamond powders. On the other hand, no continuous diamond coatings form after 12 hours MPCVD if the substrates were seeded by micro-diamond suspensions.

3. Continuous diamond coatings were successfully deposited on Al_2O_3, Al-Al_2O_3, Al-AlN and Al-Ta interlayered WC-Co cutting tools. However, the absence of an Al-based sublayer results in the formation of a graphitic layer at the interface.

4. Compared with sputtered Al_2O_3 layer, The Al layer plays the critical role in suppressing the diffusion of Co and hence limit the formation of graphite. The diamond coatings on single Al_2O_3 interlayered samples show higher graphitic carbon content than that on Al interlayered samples. A graphitic layer at the interface of diamond coating and substrate results in the delamination of diamond coating on Al_2O_3-Ta interlayered sample.

5. Even though the Al layer is able to suppress the diffusion of Co, the adhesion of diamond coating to WC-Co substrate is still significantly affected by the thermal stress and nucleation density as well as interfacial bonding. Because of the high nucleation density and the strong chemical bonding, diamond coating on Al-AlN interlayered samples shows the highest adhesion.

6. Diamond coated WC-Co sheets possess lower COF than bare WC-Co sheets regardless of whether it is rubbed against steel or alumina ball. The diamond coatings deposited on WC-Co sheets pre-etched by Murakami's solution and Caro's acid generally have lower COF than diamond coatings deposited on Al-AlN interlayered samples due to higher graphitic phase in its cauliflower structure diamond. The diamond coatings rubbing against steel ball have slightly higher COF than those rubbing against alumina ball probably because of the broken bonds between the coating and the ball.

7. The wear rate of the diamond coated WC-Co sheets is lower than that of bare WC-Co sheets, indicating the diamond coating is able to protect the WC-Co sheet and increase its wear resistance. The wear rate of the balls that rub against diamond coatings is one to two order of magnitude higher than that of bare WC-Co sheets.

5.2 Future Work

Based on this work, a few recommendations for future work are listed below:

1. Even though the adhesion of diamond coating to the WC-Co sheet has been greatly improved through the introduction of Al-AlN interlayer, the interlayer can easy be scratched off during seeding process. Therefore it is recommended to deposit some materials on top of Al layer that

have high diamond nucleation density without need for diamond seeding. Refractory metals such as Mo, W, Ta are conventionally believed to be able to increase the nucleation density. But the research in this work shows that the thermal expansion coefficient difference between them and diamond coating would introduce higher stress in the diamond coating and weaken the adhesion. Diamond-like-carbon (DLC) is another interlayer candidate material to increase the diamond nucleation density without seeding.

2. The deposition parameters of interlayer including power, bias, gas ratio, can further be optimized to deposit high dense interlayers with less defects. The Al_2O_3 layer in this work cannot efficiently suppress the diffusion of Co is probably due to the pinholes inside the layer, which provide paths for Co diffusion.

3. The COF is influenced by the orientation of the diamond crystals as well. The (100) face of diamond crystal usually presents lower COF. Therefore, it is recommended to optimize the parameters of MPCVD to control the grow orientation of diamond coatings.

LIST OF REFERENCES

[1] P. W. May, “CVD diamond: a new technology for the future.” *Endeavour*, vol. 19, no. 3, pp. 101–106, 1995.

[2] A. Hosseini and H. A. Kishawy, *Machining of Titanium Alloys*. Berlin, Heidelberg: Springer Berlin Heidelberg, 2014.

[3] M. Schwander and K. Partes, “A review of diamond synthesis by CVD processes,” *Diam. Relat. Mater.*, vol. 20, no. 9, pp. 1287–1301, Oct. 2011.

[4] R. C. Mendes De Barros, E. J. Corat, N. G. Fereira, et al. “Dispersion liquid properties for efficient seeding in CVD diamond nucleation enhancement,” *Diam. Relat. Mater.*, vol. 5, pp. 1323–1332, 1996.

[5] N. M. Everitt, R. F. Silva, J. Vieira, et al. “Friction measurements on hot filament CVD diamond films deposited on etched tungsten carbide surfaces,” *Diam. Relat. Mater.*, vol. 4, pp. 730–734, 1995.

[6] A. K. Mehlmann, A. Fayer, S. F. Dirnfeld, et al. “Nucleation and growth of diamond on cemented carbides by hot-filament chemical vapor deposition,” *Diam. Relat. Mater.*, vol. 2, no. 2–4, pp. 317–322, Mar. 1993.

[7] F. Deuerler, M. Pies, H. van den Berg, et al. “Production, Characterization, and Wear Behaviour of Plasma Jet CVD Diamond Films on Hard Metal Cutting Tools,” *Phys. Status Solidi*, vol. 154, no. 1, pp. 403–422, Mar. 1996.

[8] F. Deuerler, H. Van Den Berg, R. Tabersky, et al. “Pretreatment of substrate surface for improved adhesion of diamond films on hard metal cutting tools,” *Diam. Relat. Mater.*, vol. 5, no. 96, pp. 1478–1489, 1996.

[9] E. Cappelli, F. Pinzari, P. Ascarelli, et al. “Diamond nucleation and growth on different cutting tool materials: influence of substrate pre-treatments,” *Diam. Relat. Mater.*, vol. 5, no. 3–5, pp. 292–298, Apr. 1996.

[10] S. Silva, V. P. Mammana, M. C. Salvadori, et al. “WC-Co cutting tool inserts with diamond coatings,” *Diam. Relat. Mater.*, vol. 8, no. 10, pp. 1913–1918, Oct. 1999.

[11] T. Isozaki, Y. Saito, A. Masuda, et al. “Improvement on adhesion strength of diamond film on cemented carbide by heated intermediate layer,” *Diam. Relat. Mater.*, vol. 2, no. 8, pp. 1156–1159, May 1993.

[12] V. Kundrát, X. Zhang, K. Cooke, et al. “A novel Mo-W interlayer approach for CVD diamond deposition on steel,” *AIP Adv.*, vol. 5, p. 047130, 2015.

[13] W. C. Lai, Y. S. Wu, H. C. Chang, et al. “Enhancing the adhesion of diamond films on cobalt-cemented tungsten carbide substrate using tungsten particles via MPCVD system,” *J. Alloys Compd.*, vol. 509, no. 12, pp. 4433–4438, 2011.

[14] P. Lu, H. Gomez, X. Xiao, et al. “Coating thickness and interlayer effects on CVD-diamond film adhesion to cobalt-cemented tungsten carbides,” *Surf. Coatings Technol.*, vol. 215, pp. 272–279, 2013.

[15] F. Xu, J. H. Xu, M. F. Yuen, et al. “Adhesion improvement of diamond coatings on cemented carbide with high cobalt content using PVD interlayer,” *Diam. Relat. Mater.*, vol. 34, pp. 70–75, 2013.

[16] C. Faure, L. Teulé-gay, J. Manaud, et al. “Mechanisms of time-modulated polarized nano-crystalline diamond growth,” *Surf. Coat. Technol.*, vol. 222, pp. 97–103, 2013.

[17] K. Petrikowski, M. Fenker, J. Gäbler, et al. “Study of CrNx and NbC interlayers for HFCVD diamond deposition onto WC-Co substrates,” *Diam. Relat. Mater.*, vol. 33, pp. 38–44, 2013.

[18] J. Park, H. Lee, W. Lee, et al. “Effect of TiAl-based interlayer on the surface morphology and adhesion of nanocrystalline diamond film deposited on WC – Co substrate by hot filament CVD,” *Surf. Coat. Technol.*, vol. 258, pp. 108–113, 2014.

[19] A. Raveh, M. Weiss, M. Pinkas, et al. “Graded Al–AlN, TiN, and TiAlN multilayers deposited by radio-frequency reactive magnetron sputtering,” *Surf. Coatings Technol.*, vol. 114, pp. 269–277, 1999.

[20] R. Polini, F. P. Mantini, M. Barletta, et al. “Hot filament chemical vapour deposition and wear resistance of diamond films on WC-Co substrates coated using PVD-arc deposition technique,” *Diam. Relat. Mater.*, vol. 15, pp. 1284–1291, 2006.

[21] E. Hojman, R. Akhvlediani, a. Layyous, et al. “Diamond CVD film formation onto WC-Co substrates using a thermally nitrided Cr diffusion-barrier,” *Diam. Relat. Mater.*, vol. 39, pp. 65–72, 2013.

[22] T. Wang, L. Xiang, W. Shi, et al. “Deposition of diamond/β-SiC/cobalt silicide composite interlayers to improve adhesion of diamond coating on WC–Co substrates by DC-Plasma Assisted HFCVD,” *Surf. Coatings Technol.*, vol. 205, no. 8–9, pp. 3027–3034, Jan. 2011.

[23] H. Hei, Y. Shen, J. Ma, et al. “Effect of substrate temperature on SiC interlayers for diamond coatings deposition on WC-Co substrates,” *Vacuum*, vol. 109, pp. 15–20, 2014.

[24] A. Poulon-Quintin, C. Faure, L. Teulé-Gay, et al. “Bilayer systems of tantalum or zirconium nitrides and molybdenum for optimized diamond deposition,” *Thin Solid Films*, vol. 519, pp. 1600–1605, 2010.

[25] A. Poulon-quintin, C. Faure, L. Teulé-gay, et al. “A multilayer innovative solution to improve the adhesion of nanocrystalline diamond coatings,” *Appl. Surf. Sci.*, vol. 331, pp. 27–34, 2015.

[26] Y. S. Li and A. Hirose, “Direct coating of nanophase diamond films on steel substrate,” *Chem. Phys. Lett.*, vol. 433, no. 1–3, pp. 150–153, Dec. 2006.

[27] X. J. Li, Y. S. Li, T. J. Pan, et al. “Adhesion enhancement of diamond coating on minor Al-modified copper substrate,” *Diam. Relat. Mater.*, vol. 45, pp. 1–6, May 2014.

[28] Y. Tang, Y. S. Li, Q. Yang, et al. “Deposition and characterization of diamond coatings on WC-Co cutting tools with W/Al interlayer,” *Diam. Relat. Mater.*, vol. 19, no. 5–6, pp. 496–499, 2010.

[29] H. O. Pierson, *Handbook of Carbon, Graphite, Diamond and Fullerenes*. 1993.

[30] K. Kobashi, “Diamond – Structure and CVD Growth,” in *Diamond Films*, Elsevier, 2005, pp. 9–13.

[31] B. V. Spitsyn, L. L. Bouilov, and B. V. Derjaguin, “Vapor growth of diamond on diamond and other surfaces,” *J. Cryst. Growth*, vol. 52, no. PART 1, pp. 219–226, Apr. 1981.

[32] D. Three, “2 - Atomic and Crystal Structures of Diamond,” in *Diamond Chemical Vapor Deposition*, 1996, pp. 8–13.

[33] P. K. Bachmann, D. Leers, and H. Lydtin, “Towards a general concept of diamond chemical vapour deposition,” *Diam. Relat. Mater.*, vol. 1, no. 1, pp. 1–12, 1991.

[34] S. Matsumoto, Y. Sato, M. Tsutsumi, et al. “Growth of diamond particles from methane-hydrogen gas,” *J. Mater. Sci.*, vol. 17, no. 11, pp. 3106–3112, 1982.

[35] M. Kamo, Y. Sato, S. Matsumoto, et al. “Diamond synthesis from gas phase in microwave plasma,” *J. Cryst. Growth*, vol. 62, no. 3, pp. 642–644, Aug. 1983.

[36] R. Haubner and B. Lux, “Diamond growth by hot-filament chemical vapor deposition: state of the art,” *Diam. Relat. Mater.*, vol. 2, no. 9, pp. 1277–1294, Jul. 1993.

[37] S. Matsumoto, Y. Sato, M. Kamo, et al. “Vapor Deposition of Diamond Particles from Methane,” *Jpn. J. Appl. Phys.*, vol. 21, no. 4, pp. L183–L185, 1982.

[38] C.-P. Klages, “Chemical Vapor Deposition of Diamond,” *Appl. Phys. A*, vol. 56, no. 6, pp. 513–526, 1993.

[39] K. Kobashi, “Microwave Plasma CVD Reactors,” in *Diamond Films*, Elsevier, 2005, pp. 17–22.

[40] H. Liu and D. S. Dandy, “Diamond CVD Techniques,” in *Diamond Chemical Vapor Deposition*, Elsevier, 1995, pp. 14–45.

[41] E. Kondoh, K. Tanaka, and T. Ohta, “Homoepitaxial growth of diamond by an advanced hot-filament chemical vapor deposition method,” *J. Appl. Phys.*, vol. 74, no. 3, p. 2030, 1993.

[42] C. J. Chu, M. P. D'Evelyn, R. H. Hauge, et al. "Mechanism of diamond growth by chemical vapor deposition on diamond (100), (111), and (110) surfaces: Carbon-13 studies," *J. Appl. Phys.*, vol. 70, no. 3, pp. 1695–1705, 1991.

[43] S. Koizumi, T. Murakami, T. Inuzuka, et al. "Epitaxial growth of diamond thin films on cubic boron nitride {111} surfaces by dc plasma chemical vapor deposition," *Appl. Phys. Lett.*, vol. 57, no. 6, pp. 563–565, 1990.

[44] X. Sun, H. T. Ma, L. Z. Yang, et al. "Metal dusting, carburization and diamond deposition on Fe–Cr alloys in CH4–H2 plasma atmospheres," *Corros. Sci.*, vol. 98, pp. 619–625, Sep. 2015.

[45] H. Liu and D. S. Dandy, "Diamond Nucleation Mechanisms," in *Diamond Chemical Vapor Deposition*, Elsevier, 1995, pp. 46–78.

[46] M. Frenklach, W. Howard, D. Huang, et al. "Induced nucleation of diamond powder," *Appl. Phys. Lett.*, vol. 59, no. 5, p. 546, 1991.

[47] M. Frenklach, R. Kematick, D. Huang, et al. "Homogeneous nucleation of diamond powder in the gas phase," *J. Appl. Phys.*, vol. 66, no. 1, p. 395, 1989.

[48] F. Akatsuka and F. Shimura, "Effect of Substrate Materials on CVD Diamond Growth," in *Materials Science Monographs*, vol. 73, 1991, pp. 379–381.

[49] Z. Feng, K. Komvopoulos, I. G. Brown, et al. "Effect of graphitic carbon films on diamond nucleation by microwave-plasma-enhanced chemical-vapor deposition," *J. Appl. Phys.*, vol. 74, no. 4, pp. 2841–2849, 1993.

[50] K. V. Ravi and C. A. Koch, "Nucleation enhancement of diamond synthesized by combustion flame techniques," *Appl. Phys. Lett.*, vol. 57, no. 4, p. 348, 1990.

[51] G. Popovici and M. A. Prelas, "Nucleation and Selective Deposition of Diamond Thin Films," *Phys. Status Solidi*, vol. 132, no. 2, pp. 233–252, Aug. 1992.

[52] P. Ascarelli and S. Fontana, "Dissimilar grit-size dependence of the diamond nucleation

density on substrate surface pretreatments," *Appl. Surf. Sci.*, vol. 64, no. 4, pp. 307–311, Apr. 1993.

[53] V. G. Ralchenko, A. Saveliev, S. Voronina, et al. "Nanodiamond seeding for nucleation and growth of CVD diamond films," in *Synthesis, Properties and Applications of Ultrananocrystalline Diamond*, 2005, pp. 109–124.

[54] K. Kobashi, "Diamond Nucleation," in *Diamond Films*, Elsevier, 2005, pp. 121–153.

[55] S. Yugo, T. Kanai, T. Kimura, et al. "Generation of diamond nuclei by electric field in plasma chemical vapor deposition," *Appl. Phys. Lett.*, vol. 58, no. 10, p. 1036, 1991.

[56] B. R. Stoner, G.-H. M. Ma, S. D. Wolter, et al. "Characterization of bias-enhanced nucleation of diamond on silicon by invacuo surface analysis and transmission electron microscopy," *Phys. Rev. B*, vol. 45, no. 19, pp. 11067–11084, May 1992.

[57] X. Jiang and C. P. Klages, "Heteroepitaxial diamond growth on (100) silicon," *Diam. Relat. Mater.*, vol. 2, no. 5–7, pp. 1112–1113, 1993.

[58] B. R. Stoner and J. T. Glass, "Textured diamond growth on (100) β-SiC via microwave plasma chemical vapor deposition," *Appl. Phys. Lett.*, vol. 60, no. 6, p. 698, 1992.

[59] S. Yugo, T. Kimura, and T. Kanai, "Nucleation mechanisms of diamond in plasma chemical vapor deposition," *Diam. Relat. Mater.*, vol. 2, no. 2–4, pp. 328–332, 1993.

[60] M. Tsuda, M. Nakajima, and S. Oikawa, "The Importance of the Positively Charged Surface for the Epitaxial Growth of Diamonds at Low Pressure," *Jpn. J. Appl. Phys.*, vol. 26, no. Part 2, No. 5, pp. L527–L529, May 1987.

[61] D. Huang and M. Frenklach, "Potential energy calculations of diamond growth by methyl radicals," *J. Phys. Chem.*, vol. 95, no. 9, pp. 3692–3695, May 1991.

[62] M. Frenklach, "Monte Carlo simulation of diamond growth by methyl and acetylene reactions," *J. Chem. Phys.*, vol. 97, no. 8, p. 5794, 1992.

[63] S. J. Harris and A. M. Weiner, "Methyl radical and H-atom concentrations during diamond

growth," *J. Appl. Phys.*, vol. 67, no. 10, p. 6520, 1990.

[64] S.-T. Lee, Z. Lin, and X. Jiang, "CVD diamond films: nucleation and growth," *Mater. Sci. Eng. R Reports*, vol. 25, no. 4, pp. 123–154, 1999.

[65] M. N. R. Ashfold, P. W. May, C. A. Rego, et al. "Thin film diamond by chemical vapour deposition methods," *Chem. Soc. Rev.*, vol. 23, no. 1, p. 21, 1994.

[66] B. Sun, X. Zhang, and Z. Lin, "Growth mechanism and the order of appearance of diamond (111) and (100) facets," *Phys. Rev. B*, vol. 47, no. 15, pp. 9816–9824, Apr. 1993.

[67] G. Bräuer, B. Szyszka, M. Vergöhl, et al. "Magnetron sputtering - Milestones of 30 years," *Vacuum*, vol. 84, no. 12, pp. 1354–1359, 2010.

[68] M. Ohring, "Plasma and Ion Beam Processing of Thin Films," in *Materials Science of Thin Films*, Elsevier, 2002, pp. 203–275.

[69] P. . Kelly and R. . Arnell, "Magnetron sputtering: a review of recent developments and applications," *Vacuum*, vol. 56, no. 3, pp. 159–172, Mar. 2000.

[70] B. Window, "Charged particle fluxes from planar magnetron sputtering sources," *J. Vac. Sci. Technol. A Vacuum, Surfaces, Film.*, vol. 4, no. 2, p. 196, Mar. 1986.

[71] J. O'Brien and R. D. Arnell, "The production and characterisation of chemically reactive porous coatings of zirconium via unbalanced magnetron sputtering," *Surf. Coatings Technol.*, vol. 86–87, no. PART 1, pp. 200–206, Dec. 1996.

[72] J. Goldstein, *Scanning Electron Microscopy and X-ray Microanalysis*, vol. 44, no. 0. 2003.

[73] M. Ohring, "Characterization of Thin Films and Surfaces," in *Materials Science of Thin Films*, Elsevier, 2002, pp. 559–640.

[74] K. D. Vernon-Parry, "Scanning electron microscopy: an introduction," *III-Vs Rev.*, vol. 13, no. 4, pp. 40–44, Jul. 2000.

[75] W. Zhou and Z. L. Wang, *Scanning Microscopy for Nanotechnology*. New York, NY:

Springer New York, 2007.

[76] J. R. Ferraro, K. Nakamoto, and C. W. Brown, “Basic Theory,” in *Introductory Raman Spectroscopy*, Elsevier, 2003, pp. 1–94.

[77] S. Prawer and R. J. Nemanich, “Raman spectroscopy of diamond and doped diamond,” *Philos. Trans. R. Soc. A Math. Phys. Eng. Sci.*, vol. 362, no. 1824, pp. 2537–2565, Nov. 2004.

[78] S. J. Harris, A. M. Weiner, S. Prawer, et al. “Diamond film quality: Effects of gas phase concentrations on the Raman spectra,” *J. Appl. Phys.*, vol. 80, no. 4, p. 2187, 1996.

[79] S. Prawer, A. Hoffman, S.-A. Stuart, et al. “Correlation between crystalline perfection and film purity for chemically vapor deposited diamond thin films grown on fused quartz substrates,” *J. Appl. Phys.*, vol. 69, no. 9, p. 6625, 1991.

[80] J. W. Ager and M. D. Drory, “Quantitative measurement of residual biaxial stress by Raman spectroscopy in diamond grown on a Ti alloy by chemical vapor deposition,” *Phys. Rev. B*, vol. 48, no. 4, pp. 2601–2607, Jul. 1993.

[81] E. Anastassakis, “Strain characterization of polycrystalline diamond and silicon systems,” *J. Appl. Phys.*, vol. 86, no. 1, p. 249, 1999.

[82] V. G. Ralchenko, A. A. Smolin, V. G. Pereverzev, et al. “Diamond deposition on steel with CVD tungsten intermediate layer,” *Diam. Relat. Mater.*, vol. 4, no. 5–6, pp. 754–758, May 1995.

[83] D. Pulak, “Grazing incidence X-ray diffraction,” *Curr. Sci.*, vol. 78, no. 12, pp. 1478–1483, 2000.

[84] G. Lim, W. Parrish, C. Ortiz, et al. “Grazing incidence synchrotron x-ray diffraction method for analyzing thin films,” *J. Mater. Res.*, vol. 2, no. 04, pp. 471–477, Aug. 1987.

[85] B. N. Chapman, “Thin-film adhesion,” *J. Vac. Sci. Technol.*, vol. 11, no. 1, p. 106, Jan. 1974.

[86] M. Ohring, “Mechanical Properties of Thin Films,” in *Materials Science of Thin Films*, Elsevier, 2002, pp. 711–781.

[87] S. J. Bull, “Failure modes in scratch adhesion testing,” *Surf. Coatings Technol.*, vol. 50, no. 1, pp. 25–32, 1991.

[88] H. Ollendorf, D. Schneider, T. Schwarz, et al. “A comparative study of the mechanical properties of TiN coatings using the non-destructive surface acoustic wave method, scratch test and four-point bending test,” *Surf. Coatings Technol.*, vol. 84, no. 1–3, pp. 458–464, 1996.

[89] H. Ollendorf and D. Schneider, “A comparative study of adhesion test methods for hard coatings,” *Surf. Coatings Technol.*, vol. 113, no. 1–2, pp. 86–102, Mar. 1999.

[90] J. Gerth and U. Wiklund, “The influence of metallic interlayers on the adhesion of PVD TiN coatings on high-speed steel,” *Wear*, vol. 264, no. 9–10, pp. 885–892, 2008.

[91] J. R. Davis, “Principles of Friction and Wear,” in *Surface Engineering for Corrosion and Wear Resistance*, vol. 1, 2001, pp. 43–77.

[92] P. J. Blau, “Tribology: Friction, lubrication, and wear technology,” *ASM Handb.*, vol. 21, no. 2, pp. 122–123, 1993.

[93] R. G. Bayer, “Selection and Use of Wear Tests,” in *Mechanical Wear Fundamentals and Testing*, 2004, pp. 209–220.

[94] R. G. Bayer, “Wear Tests,” in *Mechanical Wear Fundamentals and Testing*, 2004, pp. 255–364.

[95] C. C. Chou, J. W. Lee, and Y. I. Chen, “Tribological and mechanical properties of HFCVD diamond-coated WC-Co substrates with different Cr interlayers,” *Surf. Coatings Technol.*, vol. 203, no. 5–7, pp. 704–708, 2008.

[96] Y. Fu, B. Yan, N. L. Loh, et al. “Characterization and tribological evaluation of MW-PACVD diamond coatings deposited on pure titanium,” *Mater. Sci. Eng. A*, vol. 282, no.

1–2, pp. 38–48, 2000.

[97] R. Polini, M. Barletta, and G. Cristofanilli, “Wear resistance of nano- and micro-crystalline diamond coatings onto WC-Co with Cr/CrN interlayers,” *Thin Solid Films*, vol. 519, no. 5, pp. 1629–1635, 2010.

[98] D. Durgalakshmi, M. Chandran, G. Manivasagam, et al. “Studies on corrosion and wear behavior of submicrometric diamond coated Ti alloys,” *Tribol. Int.*, vol. 63, pp. 132–140, 2013.

[99] S. Y. Luo, J.-K. Kuo, B. Yeh, et al. “The tribology of nano-crystalline diamond,” *Mater. Chem. Phys.*, vol. 72, no. 2, pp. 133–135, Nov. 2001.

[100] T. H. Huang, C.-T. Kuo, and T. S. Lin, “Tribological behaviour of chemical vapour deposition diamond films on various cutting tools,” *Surf. Coatings Technol.*, vol. 56, no. 2, pp. 105–108, Jan. 1993.

[101] H. Itoh, T. Osaki, H. Iwahara, et al. “Nucleation control of diamond synthesized by microwave plasma CVD on cemented carbide substrate,” *J. Mater. Sci.*, vol. 26, no. 14, pp. 3763–3768, Jul. 1991.

[102] A. Veillère, T. Guillemet, Z. Q. Xie, et al. “Influence of WC-Co Substrate Pretreatment on Diamond Film Deposition by Laser-Assisted Combustion Synthesis,” *ACS Appl. Mater. Interfaces*, vol. 3, no. 4, pp. 1134–1139, Apr. 2011.

[103] T. Guillemet, Z. Q. Xie, Y. S. Zhou, et al. “Stress and Phase Purity Analyses of Diamond Films Deposited through Laser-Assisted Combustion Synthesis,” *ACS Appl. Mater. Interfaces*, vol. 3, no. 10, pp. 4120–4125, Oct. 2011.

[104] M. Barletta, G. Rubino, and A. Gisario, “Adhesion and wear resistance of CVD diamond coatings on laser treated WC-Co substrates,” *Wear*, vol. 271, no. 9–10, pp. 2016–2024, 2011.

[105] A. Inspektor, E. J. Oles, and C. E. Bauer, “Theory and practice in diamond coated metal-cutting tools,” *Int. J. Refract. Met. Hard Mater.*, vol. 15, no. 1–3, pp. 49–56, Jan. 1997.

[106] M. Nesládek, K. Vandierendonck, C. Quaeyhaegens, et al., "Adhesion of diamond coatings on cemented carbides," *Thin Solid Films*, vol. 270, no. 1–2, pp. 184–188, Dec. 1995.

[107] X. Chen and J. Narayan, "Effect of the chemical nature of transition-metal substrates on chemical-vapor deposition of diamond," *J. Appl. Phys.*, vol. 74, no. 6, p. 4168, 1993.

[108] R. Polini, "Chemically vapour deposited diamond coatings on cemented tungsten carbides: Substrate pretreatments, adhesion and cutting performance," *Thin Solid Films*, vol. 515, no. 1, pp. 4–13, 2006.

[109] M. . Raghuveer, S. . Yoganand, K. Jagannadham, et al. "Improved CVD diamond coatings on WC–Co tool substrates," *Wear*, vol. 253, no. 11–12, pp. 1194–1206, Dec. 2002.

[110] M. Fraga, A. Contin, L. Rodríguez, et al. "Nano- and microcrystalline diamond deposition on pretreated WC–Co substrates: structural properties and adhesion," *Mater. Res. Express*, vol. 3, no. 2, p. 025601, 2016.

[111] R. Dumpala, M. Chandran, N. Kumar, et al. "Growth and characterization of integrated nano- and microcrystalline dual layer composite diamond coatings on WC-Co substrates," *Int. J. Refract. Met. Hard Mater.*, vol. 37, pp. 127–133, 2013.

[112] W. D. Fan, X. Chen, K. Jagannadham, et al. "Diamond-ceramic composite tool coatings," *J. Mater. Res.*, vol. 9, no. 11, pp. 2850–2867, Nov. 1994.

[113] R. Polini, F. Normand, G. Marcheselli, et al. "Early Stages of Diamond-Film Formation on Cobalt-Cemented Tungsten Carbide," *J. Am. Ceram. Soc.*, vol. 82, no. 6, pp. 1429–1435, Dec. 2004.

[114] I. Endler, A. Leonhardt, H.-J. Scheibe, et al. "Interlayers for diamond deposition on tool materials," *Diam. Relat. Mater.*, vol. 5, no. 3–5, pp. 299–303, Apr. 1996.

[115] C. R. Lin, C. T. Kuo, and R. M. Chang, "Improvement in adhesion of diamond films on cemented WC substrate with Ti–Si interlayers," *Diam. Relat. Mater.*, vol. 7, no. 11–12, pp. 1628–1632, Dec. 1998.

[116] E. Cappelli, S. Orlando, G. Mattei, et al. “Boron nitride thin films deposited by RF plasma reactive pulsed laser ablation as interlayer between WC–Co hard metals and CVD diamond films,” *Surf. Coatings Technol.*, vol. 180–181, pp. 184–189, Mar. 2004.

[117] J. P. Manaud, A. Poulon, S. Gomez, et al. “A comparative study of CrN, ZrN, NbN and TaN layers as cobalt diffusion barriers for CVD diamond deposition on WC-Co tools,” *Surf. Coatings Technol.*, vol. 202, no. 2, pp. 222–231, 2007.

[118] R. Dumpala, M. Chandran, S. Madhavan, et al. “High wear performance of the dual-layer graded composite diamond coated cutting tools,” *Int. J. Refract. Met. Hard Mater.*, vol. 48, pp. 24–30, 2015.

[119] Y. S. Li and A. Hirose, “The effects of substrate compositions on adhesion of diamond films deposited on Fe-base alloys,” *Surf. Coatings Technol.*, vol. 202, no. 2, pp. 280–287, Nov. 2007.

[120] Y. Tang, Y. S. Li, Q. Yang, et al. “Study of carbide-forming element interlayers for diamond nucleation and growth on silicon and WC-Co substrates,” *Thin Solid Films*, vol. 519, pp. 1606–1610, 2010.

[121] Y. S. Li, Y. Tang, Q. Yang, et al. “Growth and adhesion failure of diamond thin films deposited on stainless steel with ultra-thin dual metal interlayers,” *Appl. Surf. Sci.*, vol. 256, no. 24, pp. 7653–7657, Oct. 2010.

[122] Y. S. Li, Y. Tang, Q. Yang, et al. “Diamond deposition on steel substrates with an Al interlayer,” *Int. J. Refract. Met. Hard Mater.*, vol. 27, no. 2, pp. 417–420, 2009.

[123] Y. S. Li, Y. Tang, Q. Yang, et al. “Al-enhanced nucleation and adhesion of diamond films on WC–Co substrates,” *Int. J. Refract. Met. Hard Mater.*, vol. 26, no. 5, pp. 465–471, Sep. 2008.

[124] X. J. Li, L. L. He, Y. S. Li, et al. “Direct coating adherent diamond films on Fe-based alloy substrate: The roles of Al, Cr in enhancing interfacial adhesion and promoting diamond growth,” *ACS Appl. Mater. Interfaces*, vol. 5, pp. 7370–7378, 2013.

[125] X. J. Li, L. L. He, Y. S. Li, et al. “TEM interfacial characterization of CVD diamond film grown on Al inter-layered steel substrate,” *Diam. Relat. Mater.*, vol. 50, pp. 103–109, 2014.

[126] V. Edlmayr, M. Moser, C. Walter, et al. “Thermal stability of sputtered Al2O3 coatings,” *Surf. Coatings Technol.*, vol. 204, no. 9–10, pp. 1576–1581, Jan. 2010.

[127] A. C. Ferrari and J. Robertson, “Raman spectroscopy of amorphous, nanostructured, diamond-like carbon, and nanodiamond,” *Philos. Trans. R. Soc. A Math. Phys. Eng. Sci.*, vol. 362, no. 1824, pp. 2477–2512, Nov. 2004.

[128] J. B. Cui, Y. R. Ma, J. F. Zhang, et al. “Growth and characterization of diamond film on aluminum nitride,” *Mater. Res. Bull.*, vol. 31, no. 7, pp. 781–785, Jul. 1996.

[129] V. P. Godbole and J. Narayan, “Aluminum nitride buffer layer for diamond film growth,” *J. Mater. Res.*, vol. 11, no. 07, pp. 1810–1818, Jul. 1996.

[130] X. Lei, B. Shen, S. Chen, et al. “Tribological behavior between micro- and nano-crystalline diamond films under dry sliding and water lubrication,” *Tribol. Int.*, vol. 69, pp. 118–127, Jan. 2014.

[131] H. W. Xin, Z. M. Zhang, X. Ling, et al. “Composite diamond films with smooth surface and the structural influence on dielectric properties,” *Diam. Relat. Mater.*, vol. 11, no. 2, pp. 228–233, Feb. 2002.

[132] Y. P. Ma, F. H. Sun, H. G. Xue, et al. “Deposition and characterization of nanocrystalline diamond films on Co-cemented tungsten carbide inserts,” *Diam. Relat. Mater.*, vol. 16, no. 3, pp. 481–485, Mar. 2007.

[133] C. S. Abreu, M. Amaral, F. J. Oliveira, et al. “HFCVD nanocrystalline diamond coatings for tribo-applications in the presence of water,” *Diam. Relat. Mater.*, vol. 18, no. 2–3, pp. 271–275, 2009.